

**BENCHMARKING OF CRADLE CFD SOFTWARE TO
PREDICT STORE SEPARATION TRAJECTORY USING EGLIN TEST MODEL
AND
THE PREDICTION OF ONSET OF FLUTTER AND THE TRANSONIC DIP USING BSCW WING**

By
NUZA NIGAR
500079890

**SCHOOL OF ENGINEERING
(DEPARTMENT OF AEROSPACE ENGINEERING)**

**SUBMITTED
IN PARTIAL FULFILLMENT OF THE REQUIREMENT OF THE DEGREE OF
MASTER OF TECHNOLOGY**



**UNIVERSITY OF PETROLEUM AND ENERGY STUDIES
DEHRADUN
(May 2022)**

**UNDER THE GUIDANCE OF
Dr. Rajesh Yadav Dr. Karthik Sundarraj
Assistant Professor Technical Advisor
UPES Hexagon MI, India**

Prediction of Store Separation Trajectories of the Eglin Test Model using the Cradle CFD

Introduction: Prediction of Store Separation Trajectories of the Eglin Test Model using the Cradle CFD

Challenges of Store Separation in Transonic Regime

Critical to develop an accurate method of predicting the trajectory for a transonic regime

Needs to consider the compressibility effects and the strong interference flow fields that are generated between the wing and pylon and the store body

Computation cost increases due to the use of fine unstructured grids and also the use of small-time steps to achieve accuracy and stability.

Aerodynamic and physical parameters affect store separation problems.



Video: Store Separation Fatal Incidents [Video Link](#)

Introduction: Prediction of Store Separation Trajectories of the Eglin Test Model using the Cradle CFD

How CFD can help?

CFD plays a role of detecting potentially dangerous shock configurations and is part of the system of clearance for flight test and store integration

Reduce the certification time and testing cost

Avoid the fatal accidents that can occur while flight test

However, the challenge of CFD is to provide accurate data in timely manner. Accurate Prediction of the flow field is necessary for the accuracy in trajectory prediction.

The Investigated Model under Analysis: Eglin Test Model

- ❑ Delta wing with a constant NACA 64A010 airfoil section and a 45° sweep
- ❑ Pylon with an ogive-flat plate-ogive cross-section
- ❑ Finned store body with an ogive-cylinder-ogive cross-section
- ❑ On the store are four identical fins made of a clipped delta wing of a constant NACA 0008 airfoil section with a 45° sweep.
- ❑ Fins have leading and trailing edge sweep angles of 60° degrees and 0° degrees, respectively.
- ❑ The pylon and the finned body are separated by 35.6 mm.
- ❑ The length and diameter of the store are 3017.5 mm and 508.1 mm, respectively.

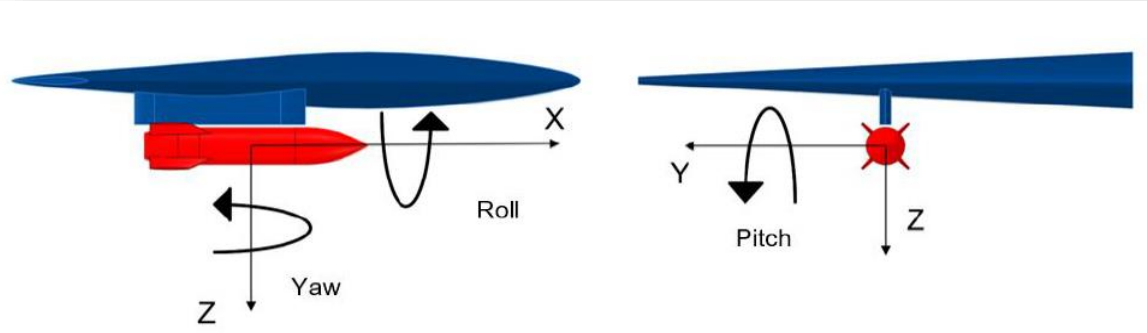


Fig. 2: The Eglin Test Case Reference

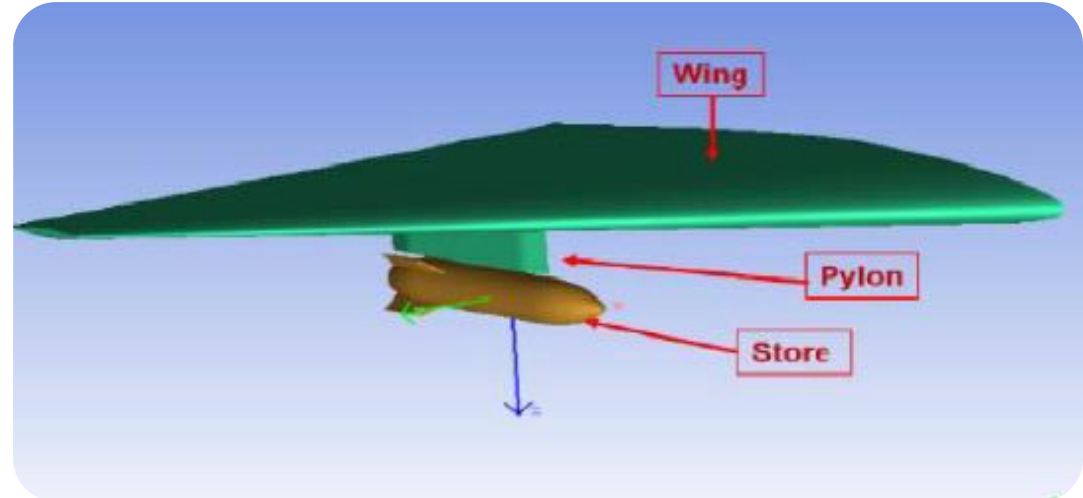


Fig.3: Geometry of the wing/pony/store

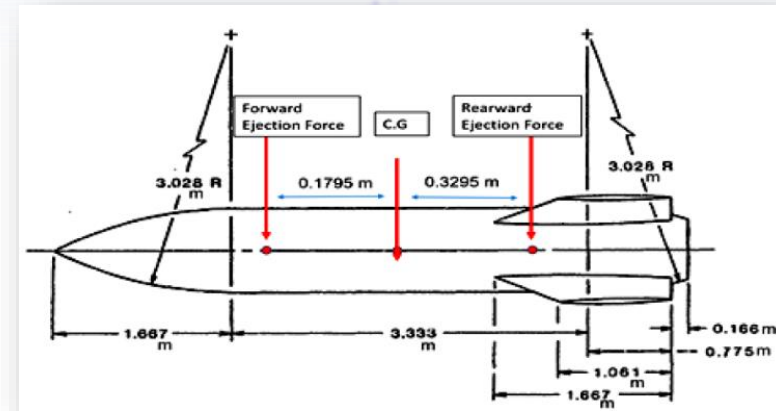


Fig.4.: Dimensions of The Store

CFD Numerics : Conservation Equations

- The geometry has been made using SOLIDWORKS. The Parasolid file was imported to be used in scFLOW. The simulation software is scFLOW and the computation was performed on the Microsoft Azure HPC platform.

Mass Conservation Equation:

$$\frac{\partial \rho}{\partial t} + \frac{\partial}{\partial x_i} \rho u_i = 0$$

Momentum Conservation Equation:

$$\frac{\partial \rho u_i}{\partial t} + \frac{\partial u_j \rho u_i}{\partial x_j} = \frac{\partial \sigma_{ij}}{\partial x_j} + \rho g_i$$

Energy Conservation Equation:

$$\frac{\partial \rho H}{\partial t} + \frac{\partial u_j \rho H}{\partial x_j} = \frac{\partial p}{\partial t} + \frac{\partial u_j p}{\partial x_j} + \sigma_{ij} \frac{\partial u_i}{\partial x_j} + \frac{\partial}{\partial x_j} K \frac{\partial T}{\partial x_j} + \dot{q}$$

Equations Of Turbulence Kinetic Energy and Turbulence Dissipation Rate (k- ϵ equations):

$$\frac{\partial \rho k}{\partial t} + \frac{\partial u_i \rho k}{\partial x_i} = \frac{\partial}{\partial x_i} \left(\frac{\mu_t}{\sigma_k} \frac{\partial k}{\partial x_i} \right) + G_S - G_{S1} - G_{S2} - G_{S3} - \rho \epsilon$$

$$\frac{\partial \rho \epsilon}{\partial t} + \frac{\partial u_i \rho \epsilon}{\partial x_i} = \frac{\partial}{\partial x_i} \left(\frac{\mu_t}{\sigma_S} \frac{\partial \epsilon}{\partial x_i} \right) + C_1 \frac{\epsilon}{k} (G_S - G_{S1} - G_{S2} - G_{S3}) - C_2 \frac{\rho \epsilon^2}{k}$$

Diffusive Species Conservation Equation

$$\frac{\partial \rho C}{\partial t} + \frac{\partial u_j \rho C}{\partial x_j} = \frac{\partial}{\partial x_j} \rho D_m \frac{\partial C}{\partial x_j} + \rho \dot{d}$$

Gas equation of state

$$p = \rho R T$$

Conservation Equations

CFD Numerics: 6 DOF Equation of Motion of Rigid Body

The Conservation Equations are coupled with the 6 DOF Equations. The 6 DOF solver computes the translational and angular motion of an object's center of gravity using the object's forces and moments.

In the inertial coordinate system, the governing equation for the translational motion of the center of gravity is solved.

$$\dot{\vec{v}}_G = \frac{1}{m} \sum \vec{f}_G$$

v_G is the translational motion of the center of gravity, m is the mass, and f_G is the gravitational force vector. Using body coordinates, the angular motion of the object, w_B , is more easily computed:

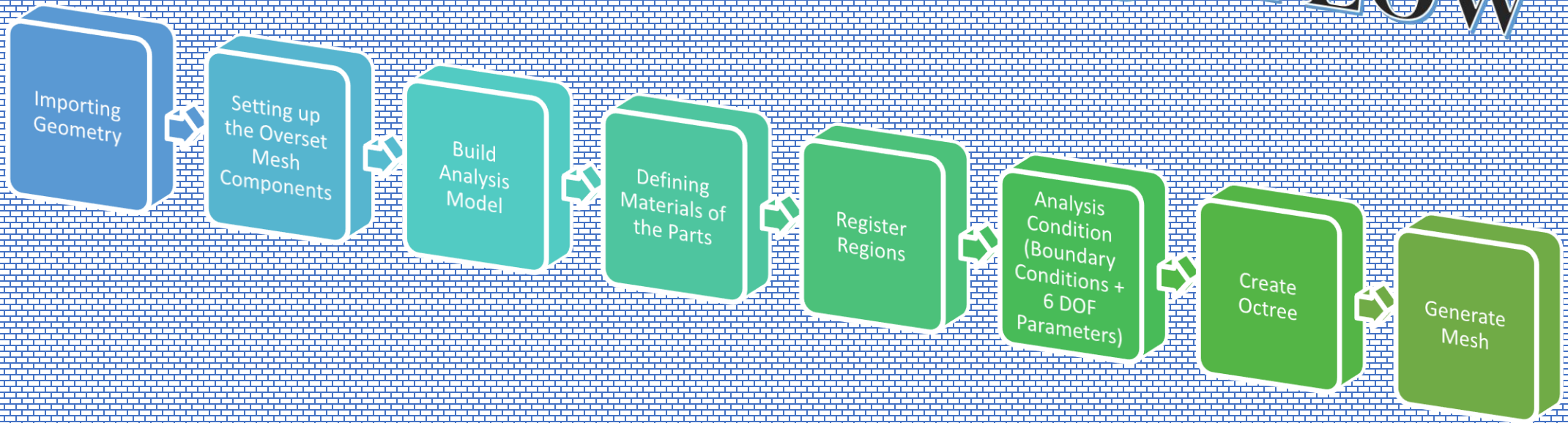
$$\dot{\vec{\omega}}_B = L^{-1} \left(\sum \vec{M}_B - \vec{\omega}_B \times L \vec{\omega}_B \right)$$

Here, where L is the inertia tensor, M_B is the moment vector of the body, and w_B is the rigid body angular velocity vector. The moments are transformed from inertial to body coordinates using given below

$$\vec{M}_B = R \vec{M}_G$$

As a result, the translational equation describes the aircraft in terms of its three translational degrees of freedom, whereas the rotational equation describes the aircraft in terms of its three rotational degrees of freedom. As a result, Newton's second law yields six equations for the six degrees of freedom of a rigid body.

Basic CFD Procedure using scFLOW



3D CAD Modelling, Overset Mesh, Build Analysis Model

3D CAD Modelling

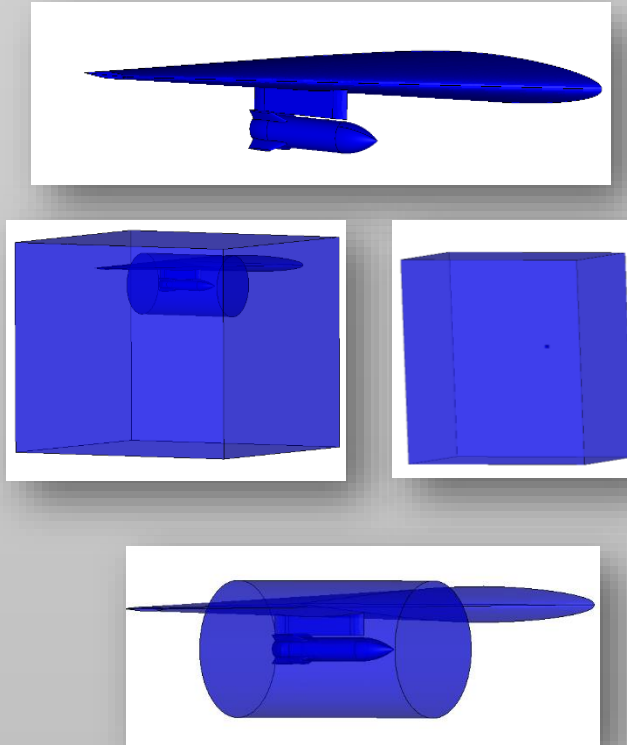


Fig. 5: Geometry

Overset Mesh

- *The overset mesh, in which multiple meshes overlap, can solve moving objects that a discontinuous mesh cannot solve or replace meshes in a portion of the analysis space with another mesh*
- *For this thesis, the two meshing units that are created in scFLOW are the background unit and the component unit. The background unit consists of the wing and the pylon, whereas the component unit consists of the missile body.*

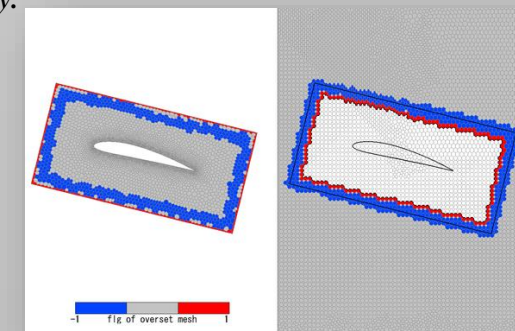


Fig. 6: Example of overset mesh

Build Analysis Model

- *By doing this, several facets are created on the model which helps in removing all the unnecessary curved edges that may interfere with the solution.*
- *Since there are two components of the overset mesh that consist of the geometry, the build analysis model will be created twice, one for each unit.*

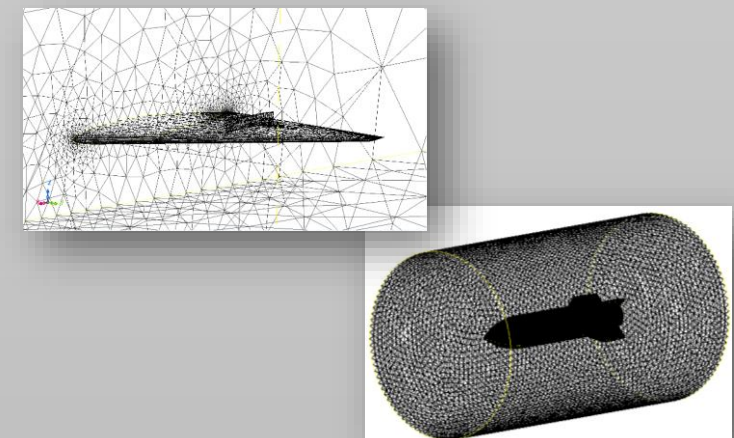


Fig. 7: Facet Creation

Discretisation in scFLOW: Octree Creation

- ❑ Elements are placed in a region to analyse physical phenomena and calculate changes in physical quantity. scFLOW includes a polyhedral mesher (arbitrary polyhedrons) to improve the cell-centered Solver's stability and calculation accuracy.
- ❑ The mesh generation involves the creation of octree and the generation of the polyhedral mesh along with the prism layers which are inserted along the wall.

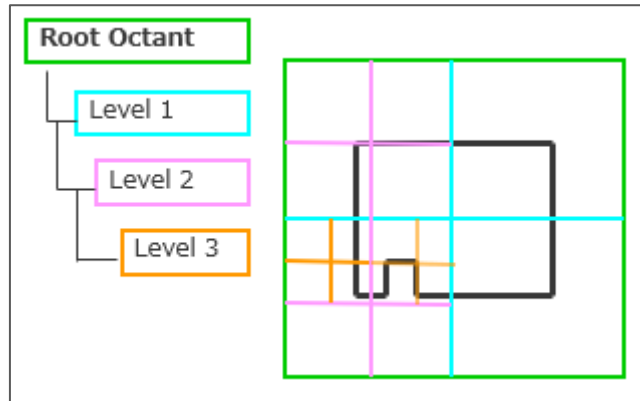


Fig. 8: Concept of Octant

Octant Size	Values
Meshing Unit [1]	
Maximum & Minimum Octant Size	12.8
Meshing Unit [2]	
Maximum & Minimum Octant Size	0.1

There are three choices that can be made to specify the octant parameter. They are as follows:

- ❑ Target a number of elements and let the octree generator decide on the sizes.
- ❑ Determine the sizes with a minimum value which will be applied to the surfaces then the octree is coarsened
- Control the octree with detailed parameters (sizes) on surfaces and volumes

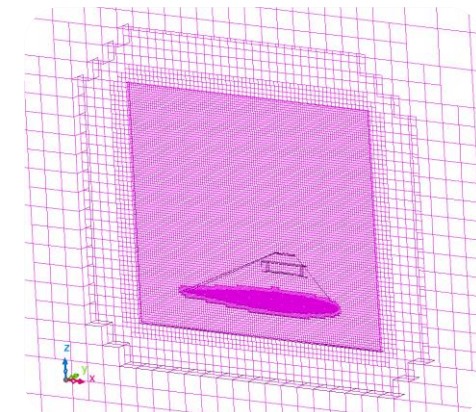


Fig. 9: Octree Creation Meshing Unit [1]

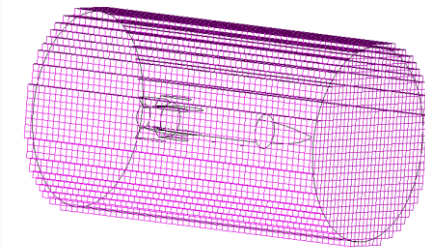


Fig. 10: Octree Creation Meshing Unit [2]

Discretisation in scFLOW: Polyhedral Mesh Generation

- ❑ The walls have been modelled as the no-slip boundary wall. For this reason, the insertion of the prism layer elements is highly recommended.
- ❑ The number of prism layers specified here is 2 and the thickness of the prism layer is 0.2.
- ❑ As the polyhedral which is an unstructured mesh is generated, the final count of the number of elements is **22,01,265**.
- ❑ The element quality is checked by judging the negative volume check. It is ideal that no negative volume element exists because such an element lowers the stability of the analysis.



Fig. 11: Polyhedron Element

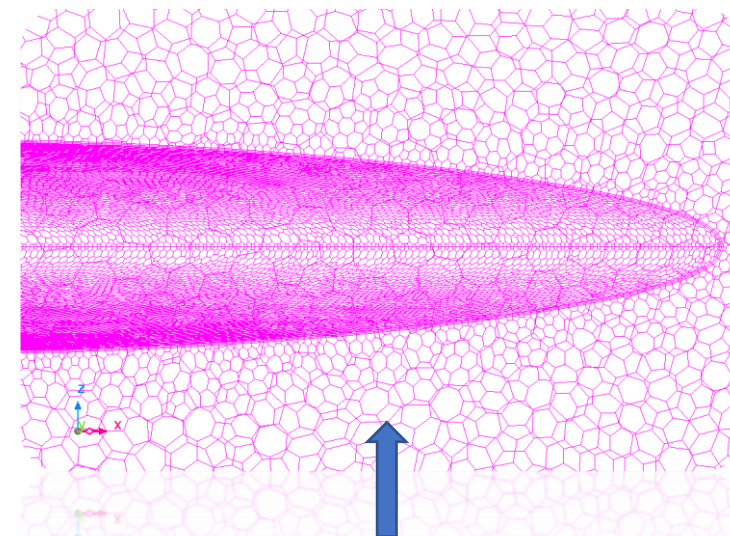
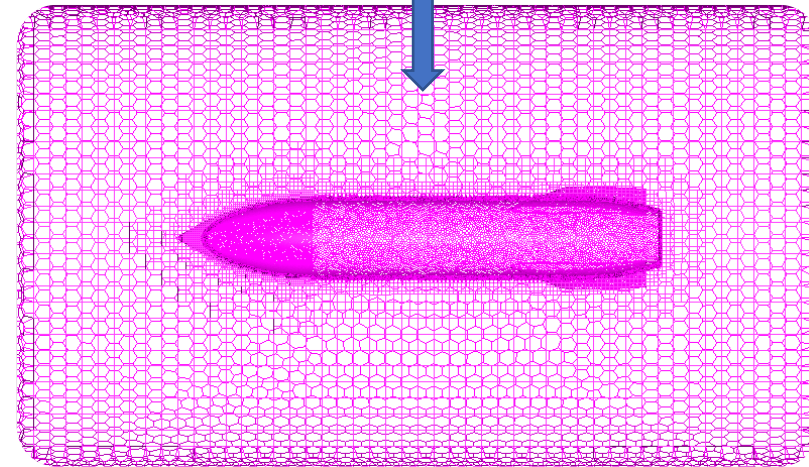
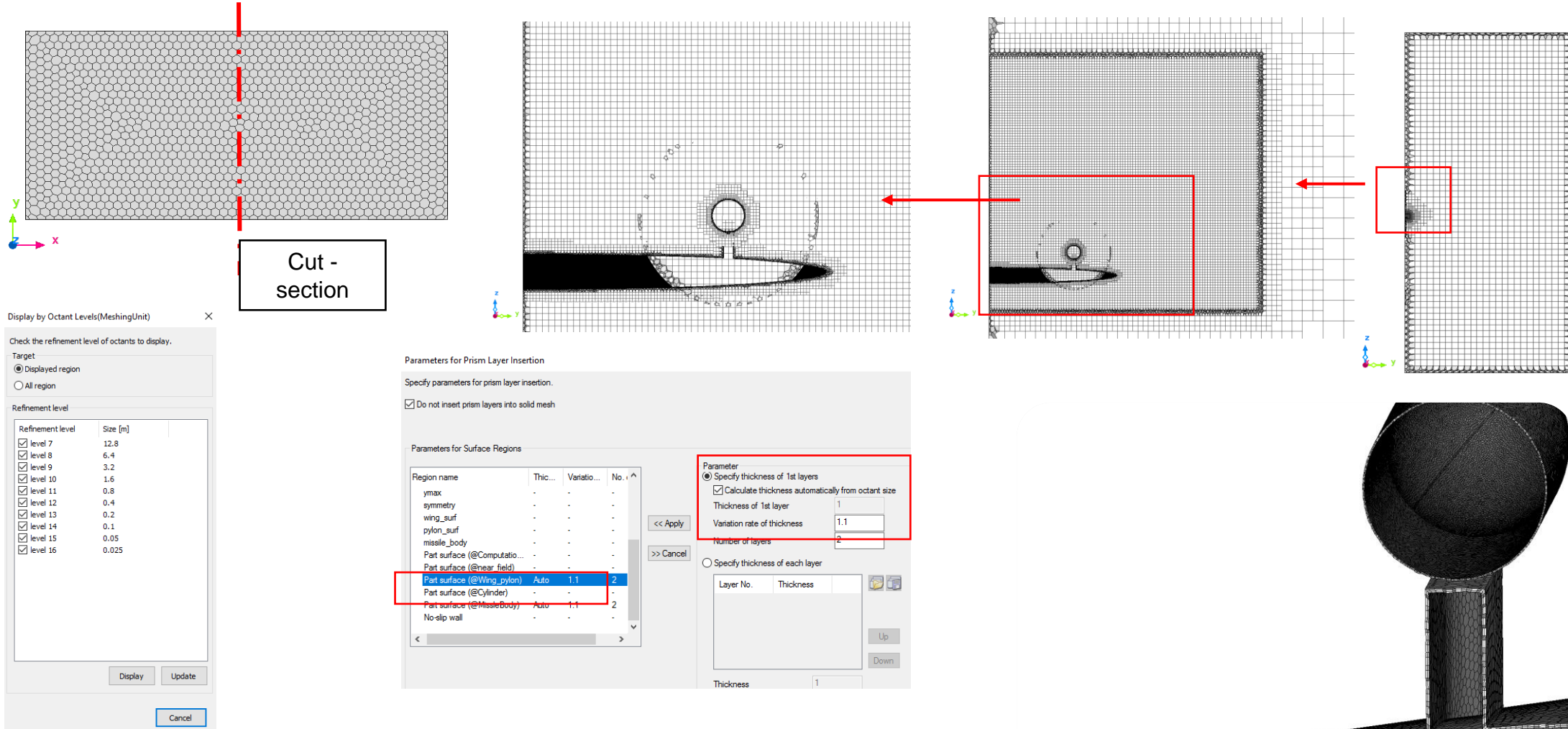


Fig. 12: Meshed Missile Body Showing Prism Layer Along the Walls

Fig. 13: Meshed Section of the Wing Showing the Prism Layer Insertion



Mesh Generation: Quality Check



Refinement level from near wall (level 16) to farfield (level 7)

Note: 1st layer is calculated automatically by the tool based on the octant size specified on the wall. It can still be captured manually based on the $y+$ and number of layers required.

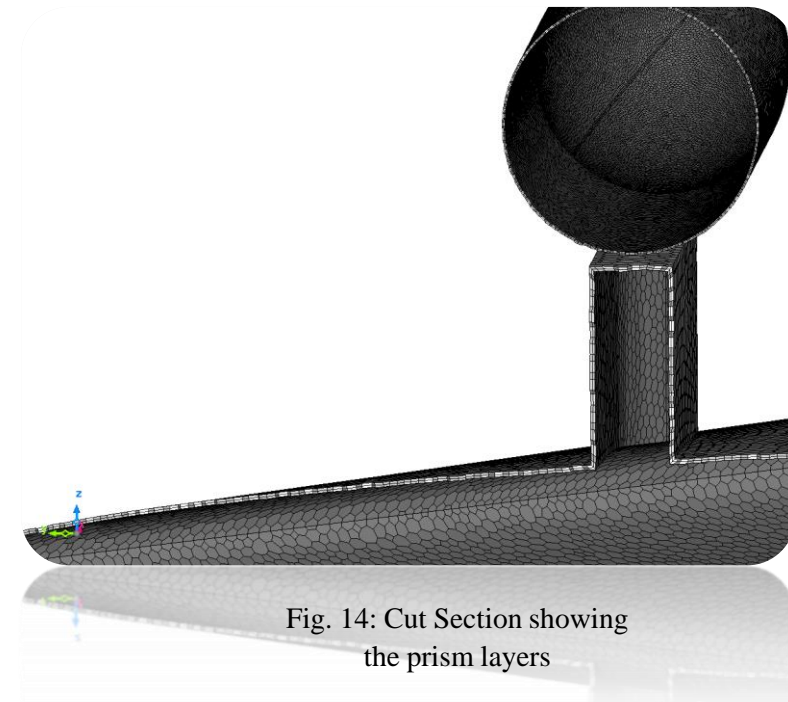


Fig. 14: Cut Section showing the prism layers

Material Specification and Registering Regions

- The wing pylon body and the missile body are modelled as an obstacle. The fluid around the obstacle is modelled as the compressible air at 20 degrees Celsius.

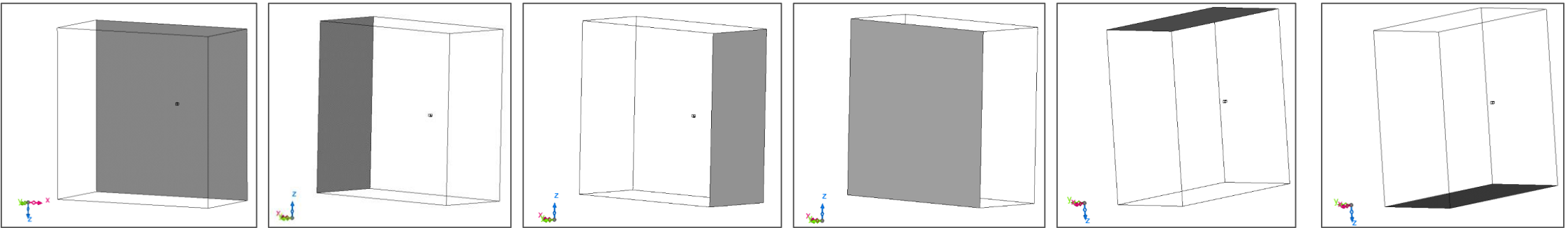


Fig. 15: Symmetry, Inlet, Outlet, Ymax, Top, Bottom Boundaries of the Domain (left to right)

- As it is known that the 6 DOF features is being applied in this problem and the importance to the ejector forces are being given, thus, to apply the ejector force, the forward and the rearward ejector surface needs to be registered. For reference to create the points at which the forward and ejector forces are applied, the point of the center of gravity is created. The coordinates of which are as follows:
 - Centre of gravity: (1.899, -3.0986, -1.57941)
 - Forward Ejector Points: (2.079, -3.0986, -1.57941)
 - Backward Ejector Points: (1.57, -3.0986, -1.57941)

Analysis Conditions and Boundary Conditions

Steady State Results are used as initialization for the Transient State Results.

Parameters	Value
Static temperature	236.7 K
Reference Pressure	36042 Pa
Mach No.	0.95
Time-step	1e-04 [s]
No. of elements	2.2 million

Turbulence Model Used	SST – K- Epsilon Model
Solver Type Used	Density Based Solver

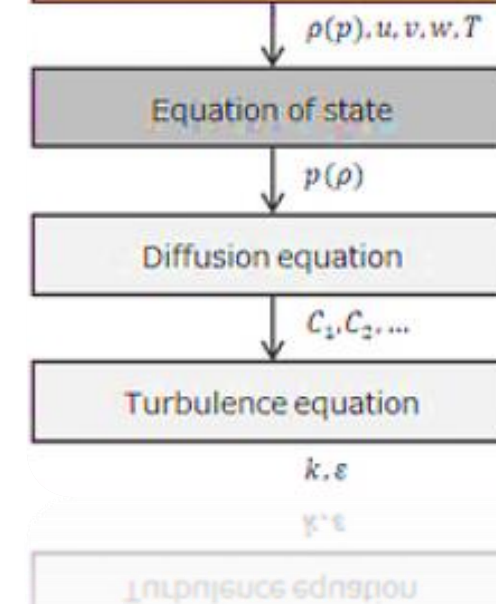
- The simulation has been performed in the transonic regime. The Mach number under consideration is 0.95.[12]
- At the inlet, the velocity component and the Mach number are specified. The velocity component is in the negative X direction as the inlet is registered in the same.
- The outlet is defined as the Static Pressure (Outflow) where the pressure value is specified as 36042 Pa.
- The top, bottom, and ymax are defined as the free slip wall boundary condition.

Density-Based Solver

Compressible flow analysis

Solve the following equations simultaneously:

- Mass conservation
- Momentum conservation
- Energy conservation



Setting Up The 6 DOF Condition

Moving Condition

Name	Moving		
Parameter	Value	Unit	Type
Motion type	6 degrees of freedom...		
Type of translation	Unrestricted		
Type of rotation	Unrestricted		
Surface region for which force is calculated	Part surface (@Missle ...)		
Specification of volume region for which mas...	Do not execute		
Mass	907.2	kg	
Centroid			
Coordinate X	1.8992	m	
Coordinate Y	-3.0986	m	
Coordinate Z	-1.57941	m	
Moment of inertia	Specify tensor		
A11	27.12	kg·m ²	
A21	0	kg·m ²	
A22	488.09	kg·m ²	
A31	0	kg·m ²	
A32	0	kg·m ²	
A33	488.09	kg·m ²	
Initial velocity	Do not set		
Initial angular velocity	Do not set		
External force	Do not set		
Normal load on surface	Set		
Forward_ejector	table	-	
Aft_ejector	table	table_2	
Friction force	Do not set		
Spring force	Do not set		
Limit translation	Set		
Minimum	0	m	
Calculate axis from part shape			
Part name	Cylinder		
		OK	Cancel

Mass	907 kg
Center of Mass	1417mm (aft of store nose)
Roll moment of inertial	27 kg·m ²
Pitch moment of inertial	488 kg·m ²
Yaw moment of inertial	488 kg·m ²
Forward ejector location	1237.5mm (aft of store nose)
Aft ejector location	1746.5mm (aft of store nose)
Forward ejector force	10.7kN
Aft ejector force	42.7kN

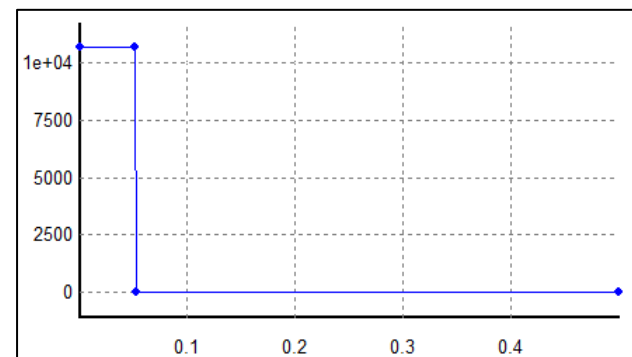


Fig. 16.: Input for Forward Ejector Force vs Time

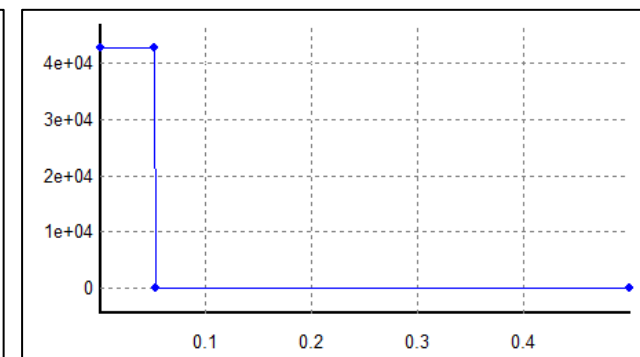


Fig. 17: Input for Aft Ejector Force vs Time

- The ejector forces were present and operate for the duration of 0.06 s after releasing the store.

Results: Attaining Accuracy through Comparisons and Testing

Linear Displacement versus Time Graph

- Figures given below depicts the trajectory of the center of gravity locations over time as compared to experimental data. When the store separates from the aircraft due to gravity and ejector forces, it begins to move backward, downward, and inward. After about $t=0.2$ seconds, the inward and backward movements begin as shown in the figure.
- Vertical displacement appears to match the experimental data very closely. This is due to the fact that the ejector and gravity forces outweigh the aerodynamic forces in this direction.

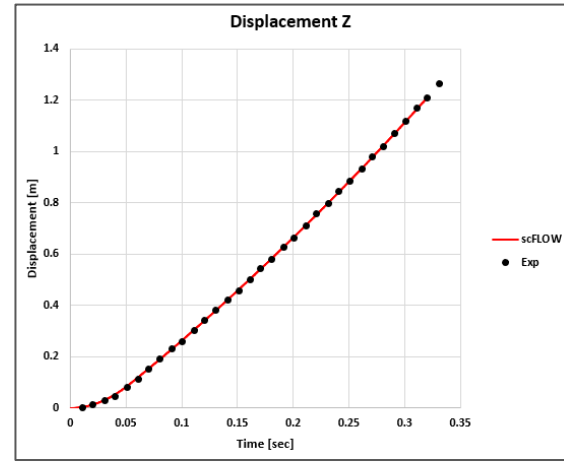
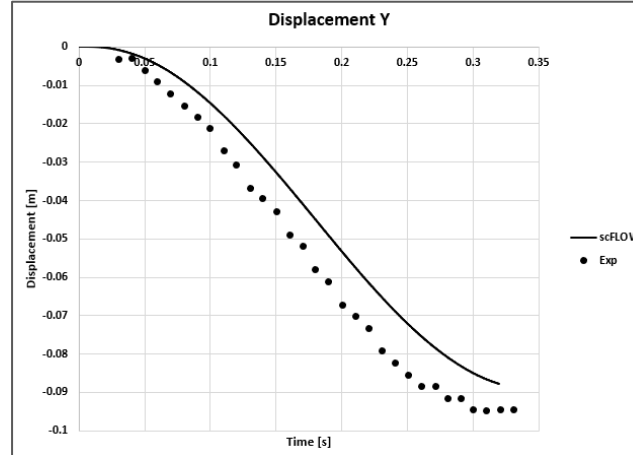
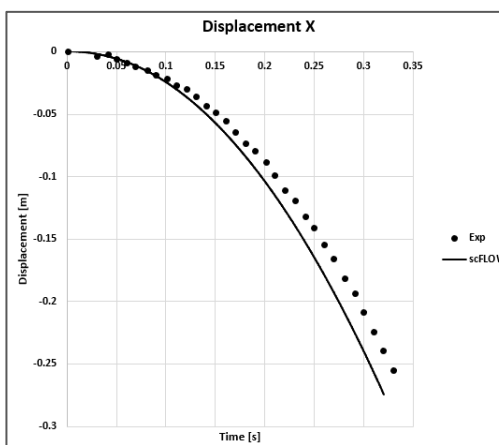


Fig. 18: Linear Displacement vs. Time in x,y and z Direction respectively

Results: Attaining Accuracy through Comparisons and Testing

Angular Displacement versus Time Graph

- Figure given below compares the trajectory for the center of gravity angular orientations with respect to time to the experimental data. Because of aerodynamic forces, the store moves in a pitch up, yaw, and right roll direction.
- The ejector forces act on the store until real-time $t=0.06$ seconds, which is the primary cause of the store pitching up. After being free of the influence of ejector forces, the motion of the store is defined by aerodynamic forces, which is why the store begins to pitch down around $t=0.19$ seconds.

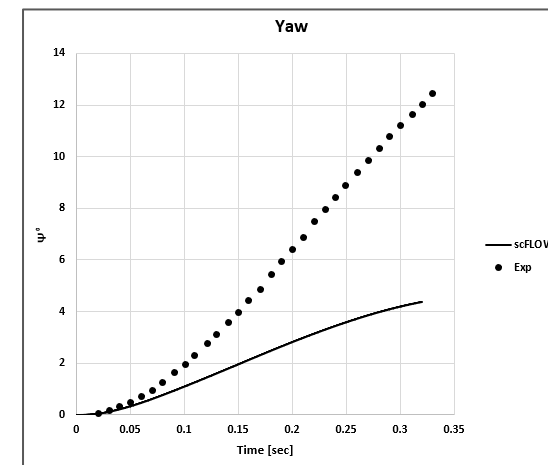
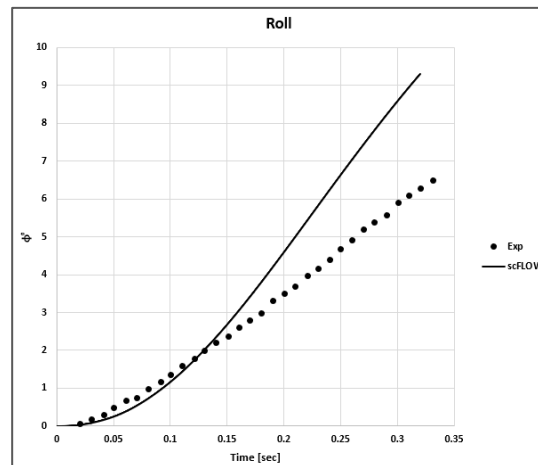
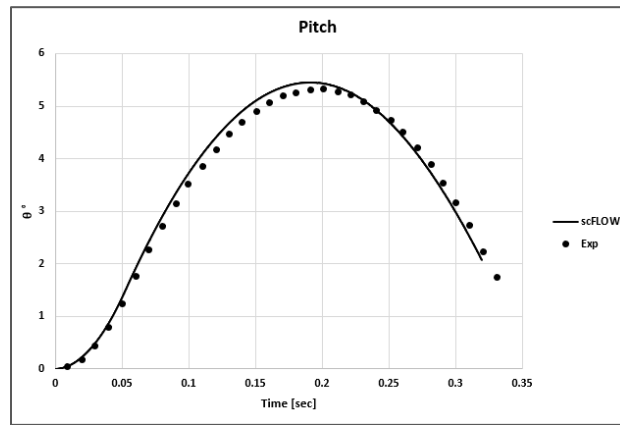


Fig. 19: Angular Displacement vs. Time in x,y and z Direction respectively

Results: Attaining Accuracy through Comparisons and Testing

Mach Contours

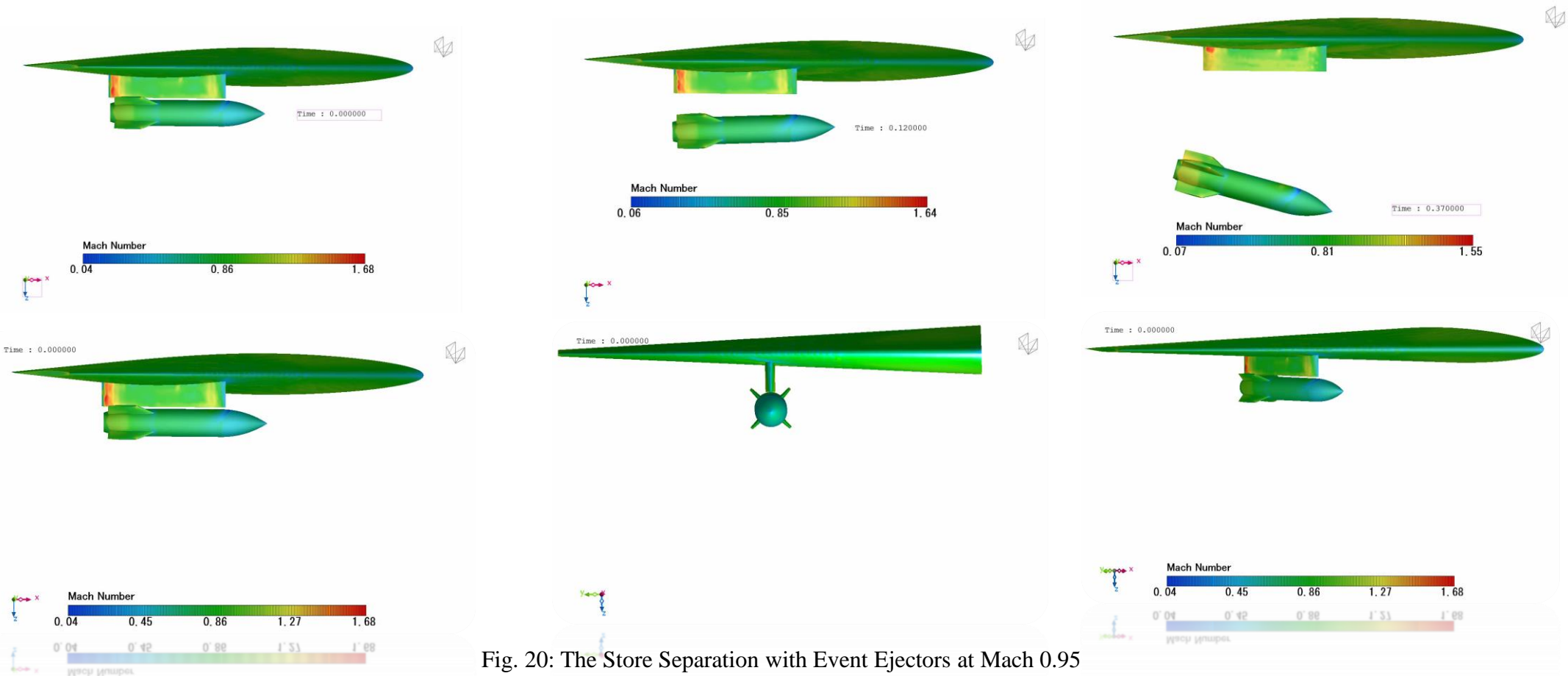


Fig. 20: The Store Separation with Event Ejectors at Mach 0.95

Results: Attaining Accuracy through Comparisons and Testing

Mach Contours

- ❑ To check if the steady state solution is required in the beginning of the transient simulation, a case was also simulated where the simulation was entirely transient and there was no steady state initialisation for the same.
- ❑ Pressure, Temperature and Velocity is initialized directly in the transient simulation The Mach contours shown in the above figure show that there was not much difference in the shock pattern observed

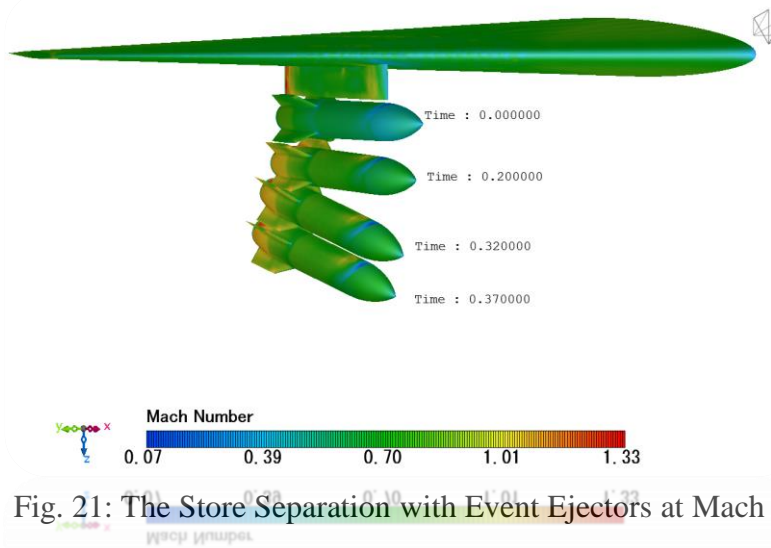


Fig. 21: The Store Separation with Event Ejectors at Mach 0.95

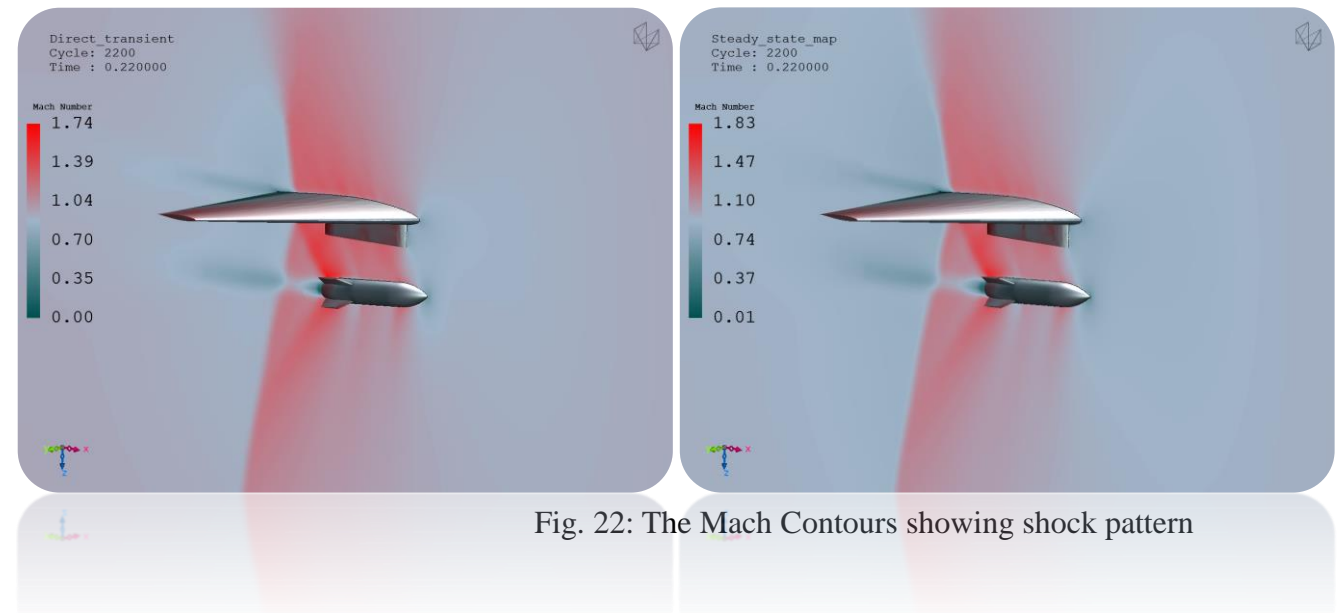


Fig. 22: The Mach Contours showing shock pattern

Future Work Recommendations

- ❑ The work on the store separation can be continued forward in many ways. A flexible Eglin case be executed to check for the structural deformations that might occur in the wing due to the weight of the missile body.
- ❑ Also further, accuracy can be improved while predicting the trajectory of separation by either refining the mesh or performing a deep study concerning the time step used.
- ❑ The same separation case can be executed using a different wing model like the Common Research Model prepared by NASA.
- ❑ Also, this case of store separation can be combined with the other case on Flutter mentioned in this thesis to check if the flutter phenomenon has any drastic consequences on store separation.

Prediction of the Onset of Flutter Boundary and the Transonic Dip using the Benchmark Supercritical Wing

Introduction: Prediction of the Onset of Flutter Boundary and the Transonic Dip using the Benchmark Supercritical Wing

What causes Flutter?

Fluttering is a common aeroelastic phenomenon. The lowest airspeed at which the structure will oscillate with sustained simple harmonic motion is defined as the flutter speed.

When there is positive feedback between the structural deflection and the force exerted by the fluid flow, an elastic structure in a fluid flow experiences dynamic instability.

When flutter occurs, the force of fluid acts as a negative damping to the structural vibration, resulting in a continuous increase in vibration magnitude.

Aircraft operating at speeds greater than flutter speeds experience a divergent unstable structural oscillation



Video: Flutter of a wing [Video Link](#)

Introduction: Prediction of the Onset of Flutter Boundary and the Transonic Dip using the Benchmark Supercritical Wing

Aeroelastic Prediction Workshop: High Angle Working Group

- ❑ Predictive use of cutting-edge coupled CFD tools (coupled: structural dynamics and unsteady aerodynamics).
- ❑ Apply to configuration and test conditions that push the modeling's range of application (i.e., physics are difficult) due to separated flow and dynamically separating flow.
- ❑ Define Mach number, angle of attack, and structural dynamic characteristics regions that require different analysis methods, grid resolution and treatment, temporal resolution, and so on.
- ❑ Examine the effect of in-tunnel effects, such as juncture flow, on unsteady characteristics such as flutter



Fig. 23: [NASA Langley Research Centre](#)

Introduction: Prediction of the Onset of Flutter Boundary and the Transonic Dip using the Benchmark Supercritical Wing

Challenges faced in Transonic Regime

- ❑ Transonic conditions are particularly difficult for computational tools to handle because strong shocks can cause separated flow.
- ❑ Many methods rely on equations that do not account for separated flow field physics.
- ❑ Flow separation can introduce flutter into a system. The most dangerous transonic flutter cases are those that occur in the transonic dip, where the onset condition (dynamic pressure at which flutter occurs) can change rapidly in terms of Mach number and angle of attack change.
- ❑ The transonic dip points are difficult to calculate and experimentally obtain.

Method of Predicting Flutter

- ❑ To understand the onset of flutter, analysis is done through the study of limit cycle oscillations. Wing limit cycle oscillations (LCO) have been observed in flight and in wind tunnel experiments on certain modern high-performance aircraft.
- ❑ It's unclear whether the physical mechanism causing this behaviour is a fluid or structural nonlinearity, or both. It has been demonstrated that an aeroelastic theoretical model with only a structural nonlinearity can accurately predict the limit cycle behaviour of a plate-like wing at zero angle of attack at low subsonic flow.
- ❑ In flight, changes in the limit cycle and flutter behaviour have been observed as the angle of attack is varied. This sensitivity to angle of attack has been attributed to fluid nonlinearity.

The Investigated Model under Analysis: BSCW Wing

- ❑ NASA SC(2)-0414 airfoil is used on the BSCW. The airfoil designation indicates that it was designed as part of the second generation of supercritical airfoils, with a design normal force coefficient of 0.4 and a thickness to chord ratio of 14 percent.
- ❑ The planform is rectangular, with wingtip caps shaped like revolution tips.
- ❑ The PAPA test was performed with several flow transition strip configurations; for these comparisons, only data from the 35 grit will be used.
- ❑ The boundary layer transition was set at a 7.5 percent chord for the OTT test using size 30 grit. Transition grit is present on both the upper and lower wing surfaces in all cases.

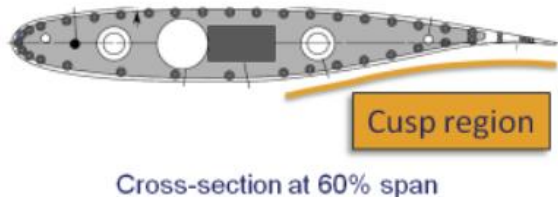


Fig.24: Cross-section of wing at 60% span[24]

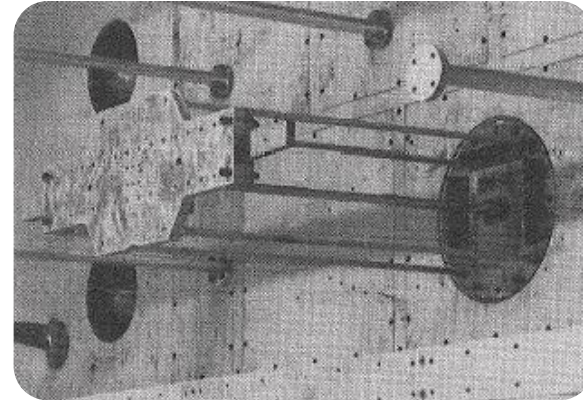


Fig. 25: Photograph of PAPA[25]



Fig. 26: Experimental Setup of BSCW Wing[26]

CFD Numerics : Conservation Equations

- The geometry has been made using SOLIDWORKS. The Parasolid file was imported to be used in scFLOW. The simulation software is scFLOW for CFD and the MSC Nastran for Computational Structural Mechanics and the computation was performed on the Microsoft Azure HPC platform.

Mass Conservation Equation:

$$\frac{\partial \rho}{\partial t} + \frac{\partial}{\partial x_i} \rho u_i = 0$$

Momentum Conservation Equation:

$$\frac{\partial \rho u_i}{\partial t} + \frac{\partial u_j \rho u_i}{\partial x_j} = \frac{\partial \sigma_{ij}}{\partial x_j} + \rho g_i$$

Energy Conservation Equation:

$$\frac{\partial \rho H}{\partial t} + \frac{\partial u_j \rho H}{\partial x_j} = \frac{\partial p}{\partial t} + \frac{\partial u_j p}{\partial x_j} + \sigma_{ij} \frac{\partial u_i}{\partial x_j} + \frac{\partial}{\partial x_j} K \frac{\partial T}{\partial x_j} + \dot{q}$$

Equations Of Turbulence Kinetic Energy and Turbulence Dissipation Rate (k- ϵ equations):

$$\frac{\partial \rho k}{\partial t} + \frac{\partial u_i \rho k}{\partial x_i} = \frac{\partial}{\partial x_i} \left(\frac{\mu_t}{\sigma_k} \frac{\partial k}{\partial x_i} \right) + G_S - G_{S1} - G_{S2} - G_{S3} - \rho \epsilon$$

$$\frac{\partial \rho \epsilon}{\partial t} + \frac{\partial u_i \rho \epsilon}{\partial x_i} = \frac{\partial}{\partial x_i} \left(\frac{\mu_t}{\sigma_S} \frac{\partial \epsilon}{\partial x_i} \right) + C_1 \frac{\epsilon}{k} (G_S - G_{S1} - G_{S2} - G_{S3}) - C_2 \frac{\rho \epsilon^2}{k}$$

Diffusive Species Conservation Equation

$$\frac{\partial \rho C}{\partial t} + \frac{\partial u_j \rho C}{\partial x_j} = \frac{\partial}{\partial x_j} \rho D_m \frac{\partial C}{\partial x_j} + \rho \dot{d}$$

Gas equation of state

$$p = \rho R T$$

Conservation Equations

CFD Numerics : Differential Non-linear Equation Valid For a Dynamic System With Large Displacements

The CSM solver uses a differential non-linear equation valid for a dynamic system with large displacements based on the Finite Element Method.

The Nastran file is defined to model the structural shape, mesh, thickness distribution of the shell elements, material, and displacement constraint.

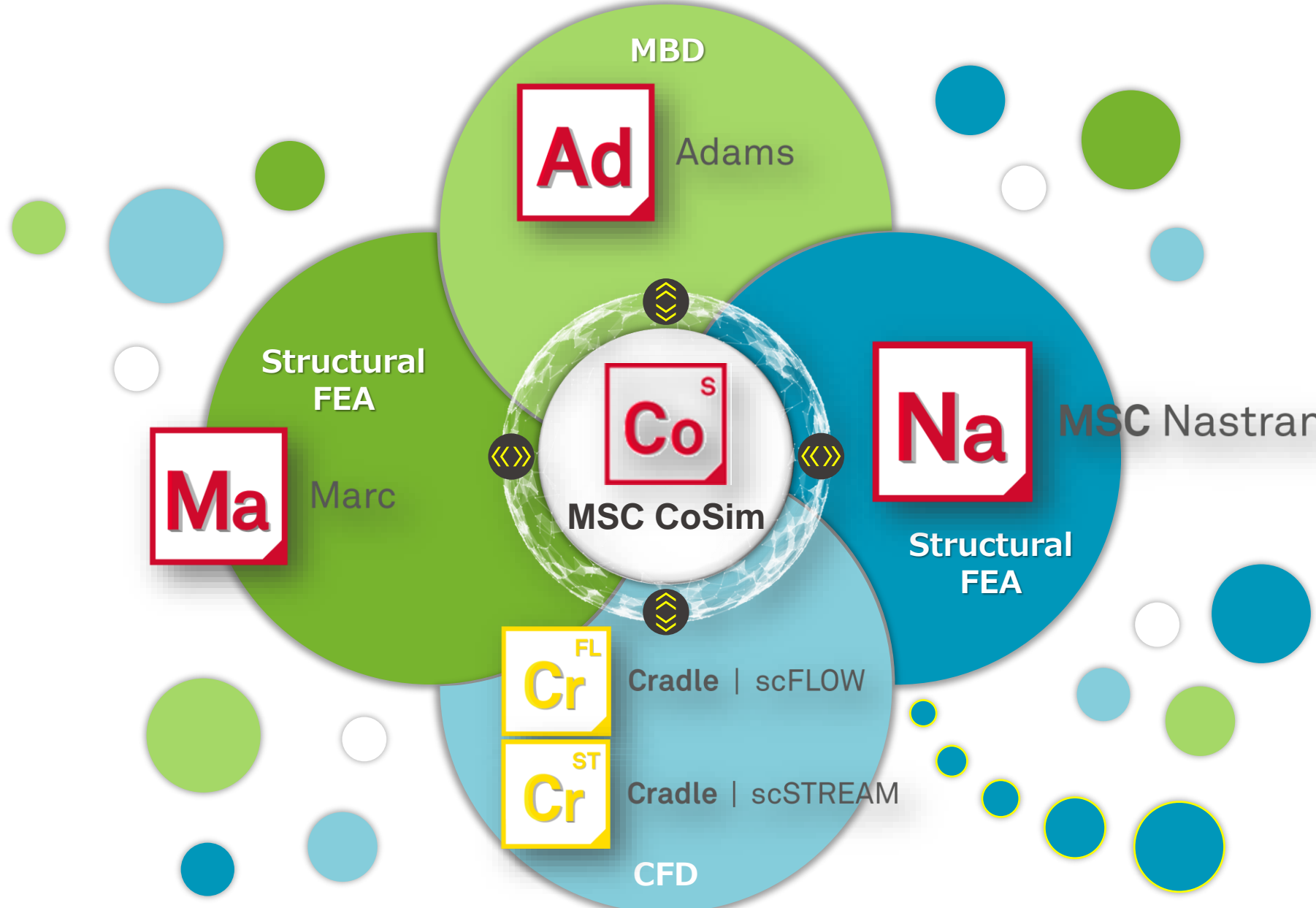
The governing equations for the CSM analysis are given below.

The equation of motion of a structure is given by the Equation below.

$$Ma + Cv + Ku = F$$

CFD – CSM – Cosimulation Flow Process

FSI analysis was done using MSC Nastran, scFLOW and MSC CoSim



- MSC CoSim can perform cosimulation by combining many software like MARC, ADAMS and MSC Nastran.
- For this case, the FSI analysis is performed using scFLOW and MSC Nastran.

Computational Fluid Dynamics: scFLOW Process

3D CAD Modelling

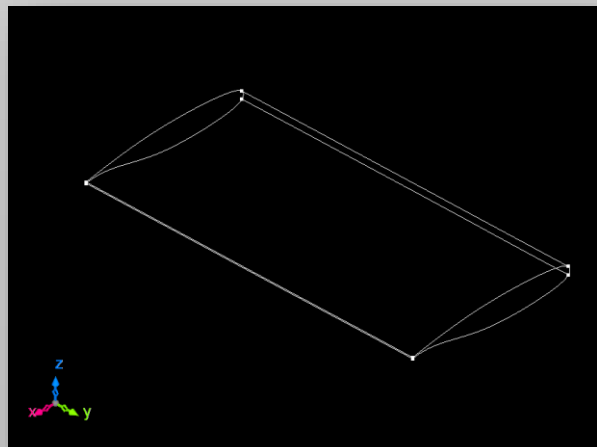


Fig. 27: Geometry of BSCW Wing

Build Analysis Model

- By doing this, several facets are created on the model which helps in removing all the unnecessary curved edges that may interfere with the solution.

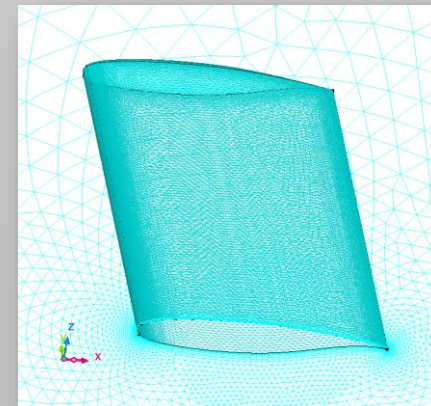


Fig. 28: Triangular Faceter

Discretisation in scFLOW: Octree Creation

There are three choices that can be made to specify the octant parameter. They are as follows:

- Target a number of elements and let the octree generator decide on the sizes.
- Determine the sizes with a minimum value which will be applied to the surfaces then the octree is coarsened
- Control the octree with detailed parameters (sizes) on surfaces and volumes

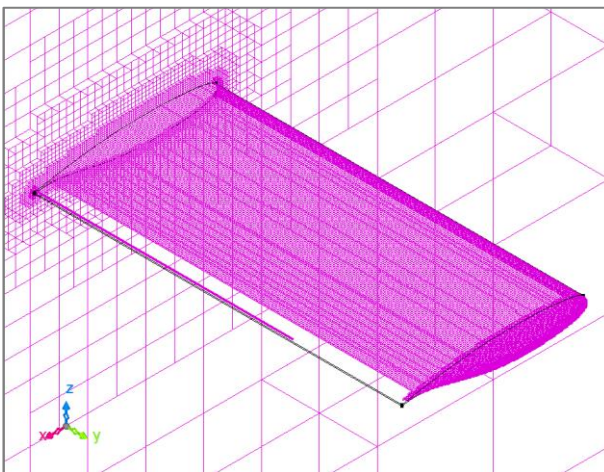


Fig.29: Octree Creation around the wing wall

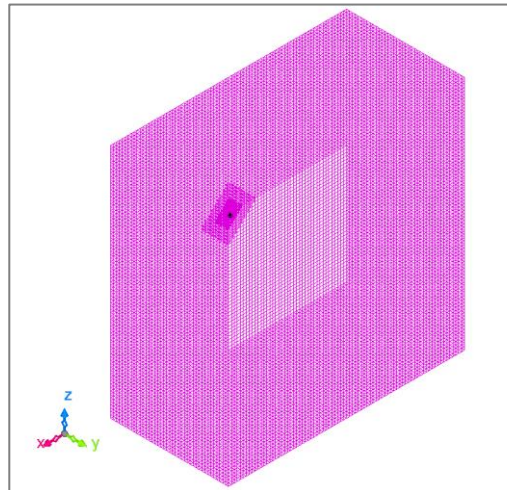


Fig. 30: Octree Creation in the entire domain

Octant Size	Values
Basic Octant Sizing	
Maximum & Minimum Octant Size	2.048
Region Octant Sizing	

Region	Size	Influence Range
Wall	0.32	8
Wall Trailing Edge	0.004	2
Wall Leading Edge	0.004	2
Wall tip	0.004	2
Wall Upper surface	0.008	2
Wall Lower surface	0.008	2

Discretisation in scFLOW: Polyhedral Mesh Generation

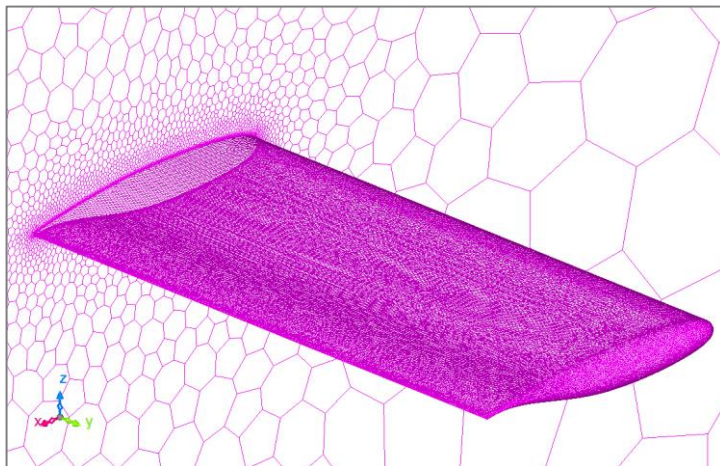
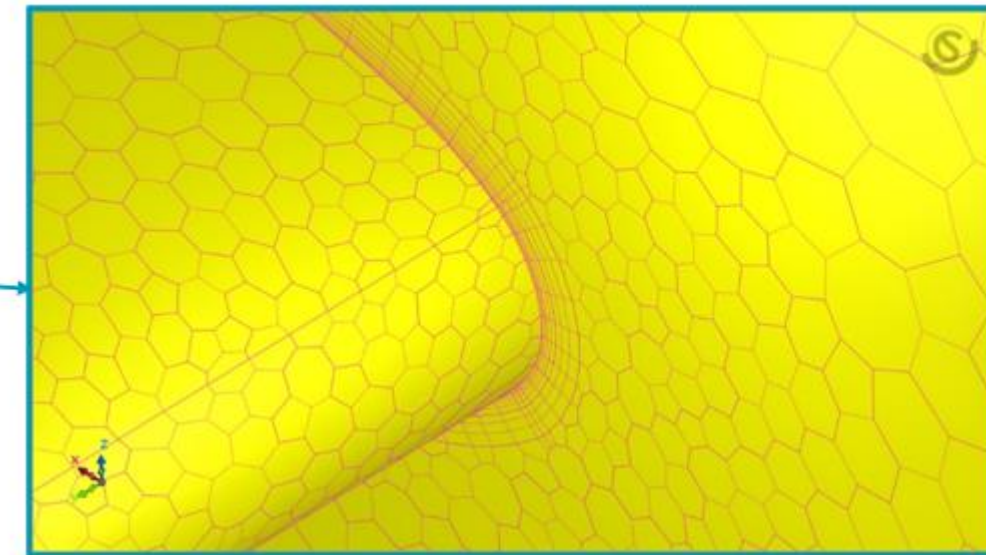
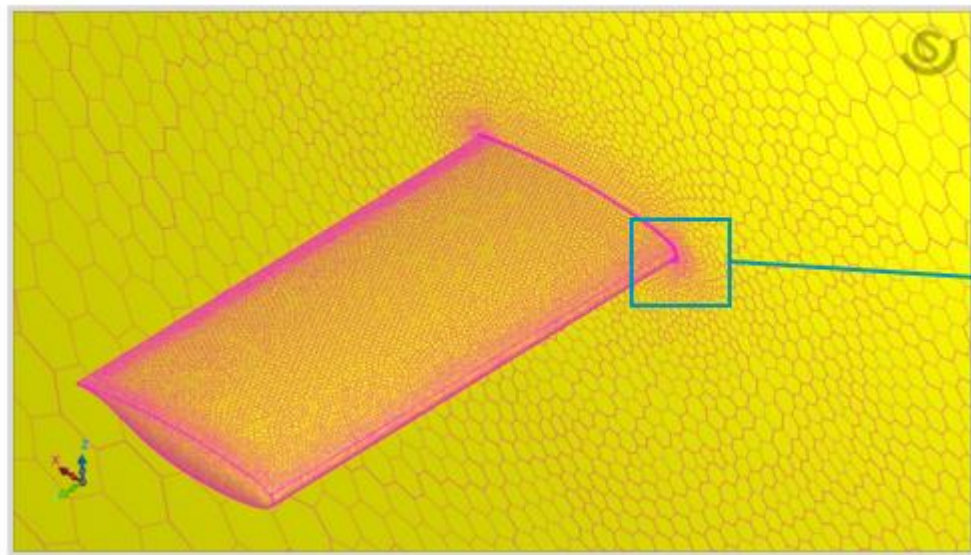


Fig. 31: Polyhedral Mesh Generation

===== GPH FILE GEOMETRY =====

SPACE DIMENSION	=	3
TOTAL NODE NUMBER	=	1818706
TOTAL FACE NUMBER	=	2398952
TOTAL ELEMENT NUMBER	=	422147

Material Specification and Registering Regions

- The material specified for the fluid domain is the compressible air at 20 degrees Celsius. The wing body is specified as an obstacle. The symmetrical computational domain is considered

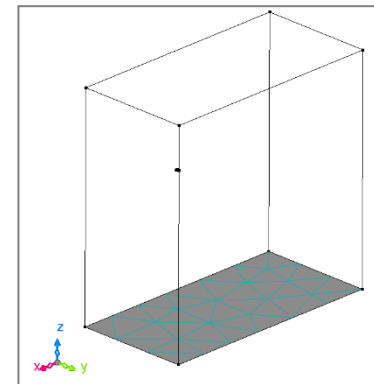
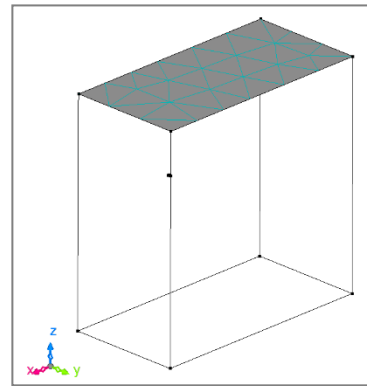
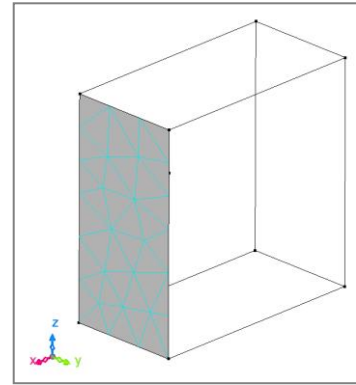
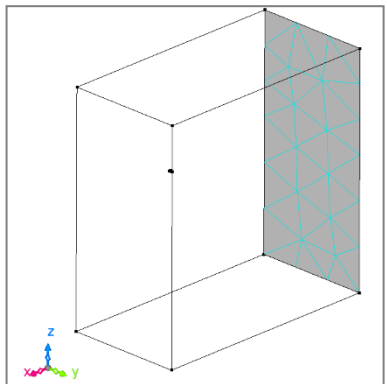
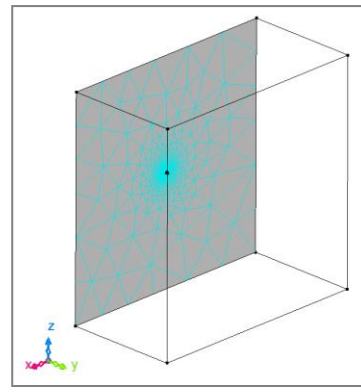
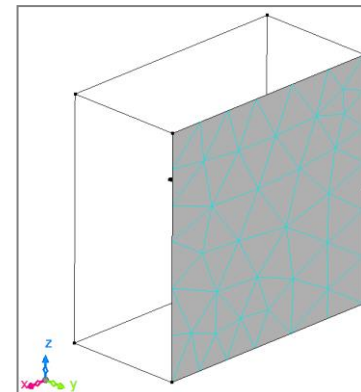


Fig. 15: Symmetry, Inlet, Outlet, Ymax, Top, Bottom Boundaries of the Domain (left to right)



Analysis Conditions and Boundary Conditions

Steady State Results are used as initialization for the Transient State Results.

Parameters	Value
Time-step	0.0002
No. of elements	422417
Turbulence Model Used	SST – K- Omega Model
Solver Type Used	Density Based Solver

- To predict the flutter dynamics pressure at various Mach numbers, several cases were executed. The flow boundary conditions depend upon the values of the components of velocity calculated which are the Vx and Vz.
- The temperature values are also calculated as well as the pressure values. Table given aside shows all the cases that have been executed. This table shows the parameters under consideration used for the calculation of Vx, Vz, Temperature T, and Pressure P.
- Uniform flow is assumed across the boundaries. The symmetrical boundary condition is applied to the symmetry boundary and the Ymax, the top surface of the computational domain and the bottom as well is subject to the uniform flow condition.
- No-Slip wall boundary condition is applied to the wall of the wing.

case	M	Dynamic Pressure (Pa)	psf	Vx	Vz	T	P
1	0.7	6300	131.5781	91.59439	8.013471	184.7803	23041.45
2		6400	133.6667	93.04827	8.140669	190.6929	23407.19
3		6200	129.4896	90.14051	7.886273	178.9608	22675.72
4		6250	130.5339	94.50215	8.267867	196.6986	23772.93

case	M	Dynamic Pressure (Pa)	psf	Vx	Vz	T	P
1	0.75	5800	121.1354	84.32499	7.377481	136.4282	18478.68
2		5900	123.224	85.77887	7.504679	141.1732	18797.28
3		5700	119.0469	82.87111	7.250283	131.7643	18160.08
4		5750	120.0911	83.59805	7.313882	134.0861	18319.38

case	M	Dynamic Pressure (Pa)	psf	Vx	Vz	T	P
1	0.8	1900	33	22.97202	2.009791	8.898818	4424.419
2		1700	35.50520778	24.71595	2.162365	10.30122	4760.301
3		1800	37.59374941	26.16983	2.289563	11.54877	5040.318
4		1850	38.63802023	26.89677	2.353162	12.19928	5180.327

case	M	Dynamic Pressure (Pa)	psf	Vx	Vz	T	P
1	0.85	3800	79.36458209	55.24735284	4.833517063	45.59310293	9425.63732
2		3700	77.27604046	53.79353077	4.706324114	43.22512953	9177.603726
3		3750	78.32031128	54.52047038	4.769923088	44.40126983	9301.625398
4		5745.96	120	83.53460729	7.30833115	104.2339205	14251.66767

case	M	Dynamic Pressure (Pa)	psf	Vx	Vz	T	p
1	0.8	4788.3	100	69.61217	6.090276	8.171550E+01	13407.33
2		5745.96	120	83.53461	7.308331	1.176703E+02	16088.80
3		6703.62	140	97.45704	8.526386	1.601624E+02	18770.26

Analysis Conditions and Boundary Conditions

Excel calculator to calculate Vx, Vz, T and P

AoA	5					
Mach	0.85					
R	83.66297416 <small>(=a*a/T/γ)</small>					
γ	1.116					
q(psf) – Dynamic Pressure	3800	q(Pa)	1psf=	47.88026	Pa	
μ(slug/ft³-s) - Viscosity	2.59E-07	μ(Pa-s)		5745.631		
Reynolds No.	4.49E+06					
Prandtl Number	6.74E-01					
Chord	0.4064		0.24384	0.48768		
Vx	2.645263E+03					
Vz	2.314305E+02					
V	2.655367E+03					
ρ	5.16E-02					
a	3.123961E+03					
T	1.045235E+05					
p	451302.81					
Cp	804.89551		1slug=	14.5939	kg	
k	1.480934E-02		1ft=	0.3048	m	
			87.913	F	=	304.2128
		ref		R	=	84.21945

The calculator above has been prepared using the basic formulas given below:

For ideal gas

$$P = \rho R T$$

Speed of sound in air:

$$a = \sqrt{\gamma RT}$$

Mach Number:

$$M = V/a$$

Dynamic Pressure:

$$q = 0.5 \rho a^2$$

Reynolds Number:

$$R_e = \frac{\rho V L}{\mu}$$

Prandtl Number:

$$Pr = Cp\mu/k$$

Computational Structural Mechanics: Nastran Process

- ❑ The Nastran software is used to prepare the structures of the wing as shown in figure given below.
- ❑ The grid points 13, 14 and 15 which is at the leading edge of the wing to the trailing edge of the wing chosen to map the displacement at these points.
- ❑ It involves making grid points at which the equations will be solved. The file prepared for this thesis uses the CQUAD elements. [38]
- ❑ The material is specified with its properties such as the Young's Modulus and Poisson ratio.
- ❑ The element properties and the boundary conditions are specified.
- ❑ The stiffness matrix is solved in Nastran to get the displacement
- ❑ The FEM Model looks like the Figure given below. Since this thesis focuses on the CFD aspect of the problem, the details on the structure side are limited.

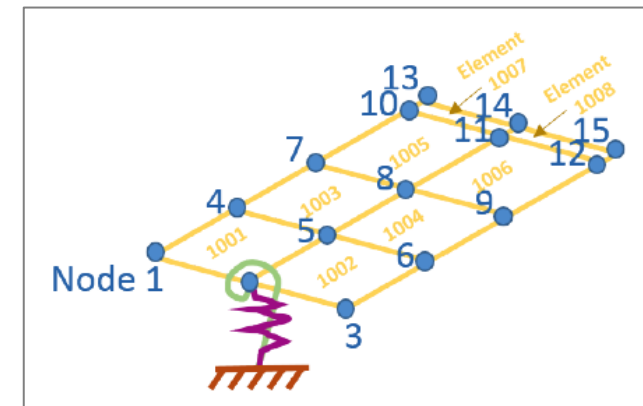
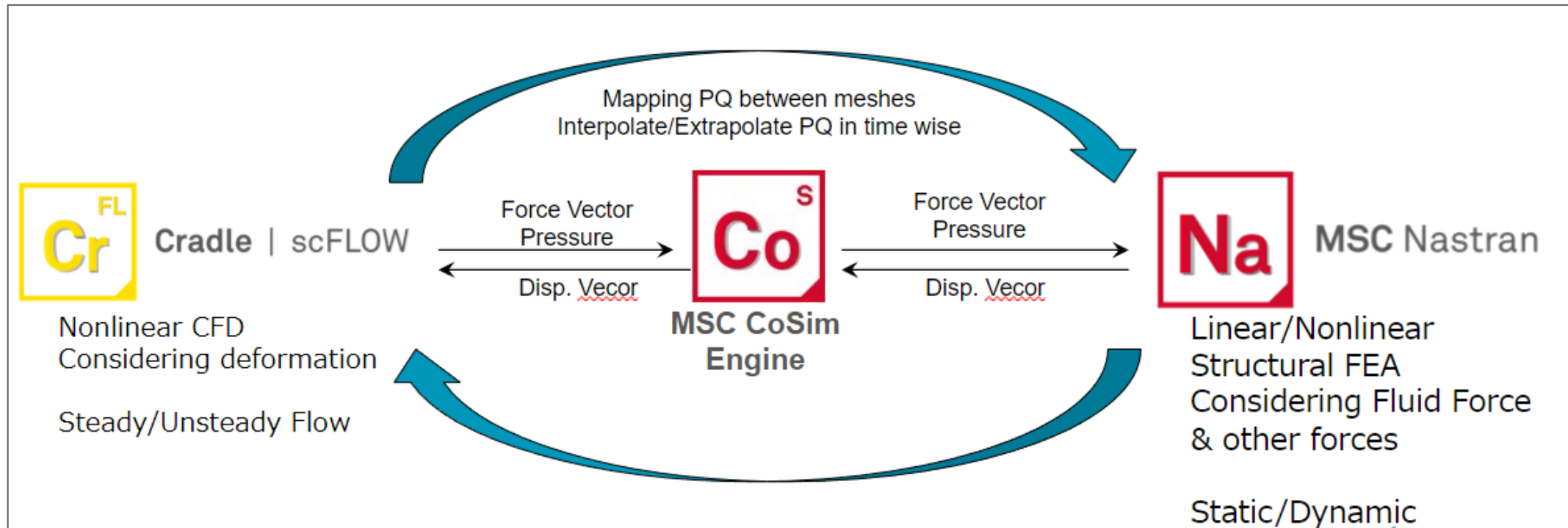


Fig. 32: FEM Model [37]

Cosimulation using MSC CoSim



Through the application of MSC CoSim, in this analysis, the flow field and the temperature field from the fluid analysis in scFLOW are mapped to structural mesh as pressure load in MSC Nastran. scFLOW then receives the displacement loads from MSC Nastran and this way two-way coupling is established.

Results: Onset of Flutter Boundary

Mach Number	Experimental Dynamic Pressure Values	CFD Dynamic Pressure Values attained
0.7	6300	6250
0.75	5800	5750
0.8	1900	1700
0.85	3800	3800

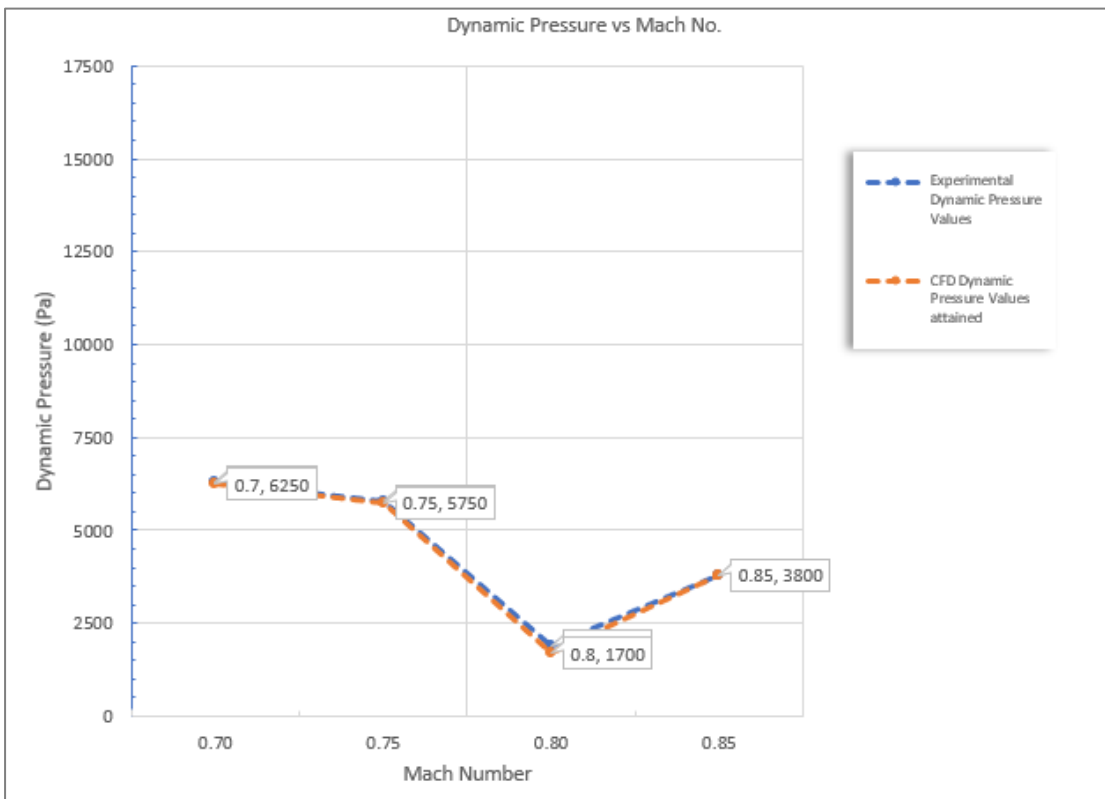


Fig. 33: CoSim vs Experimental Flutter Dynamic Pressure obtained

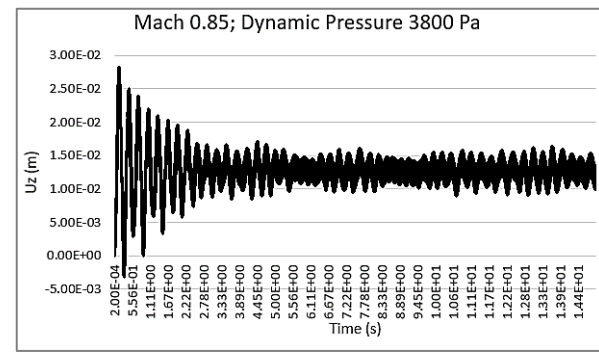
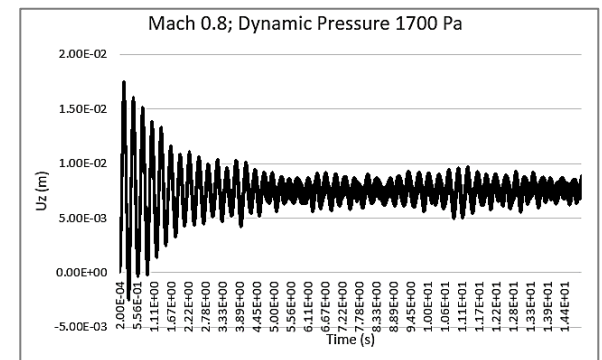
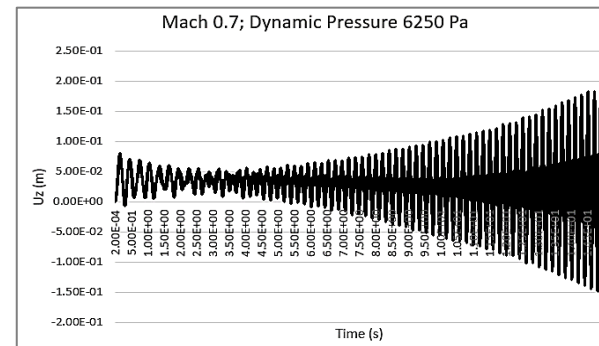
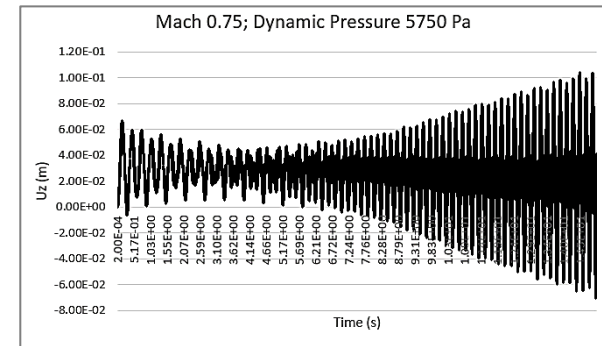


Fig. 34: Linear Displacement Graphs

Results: Transonic Dip at Mach 0.8

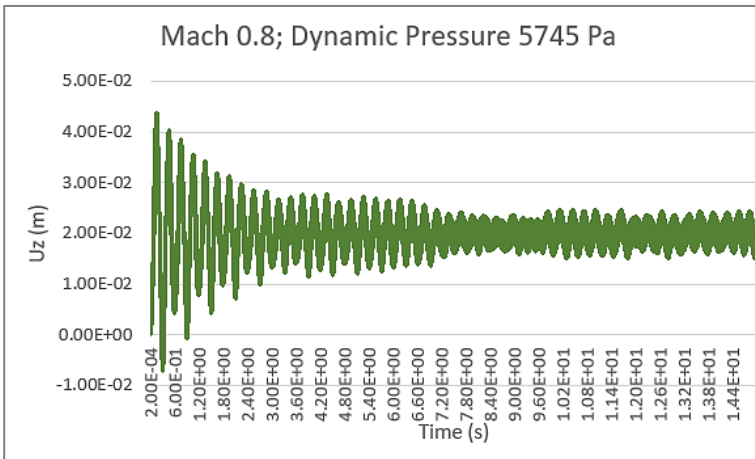


Fig. 35: Displacement Graph for Mach 0.8 and
Flutter Dynamic Pressure 5745 Pa (AoA 5
degrees)

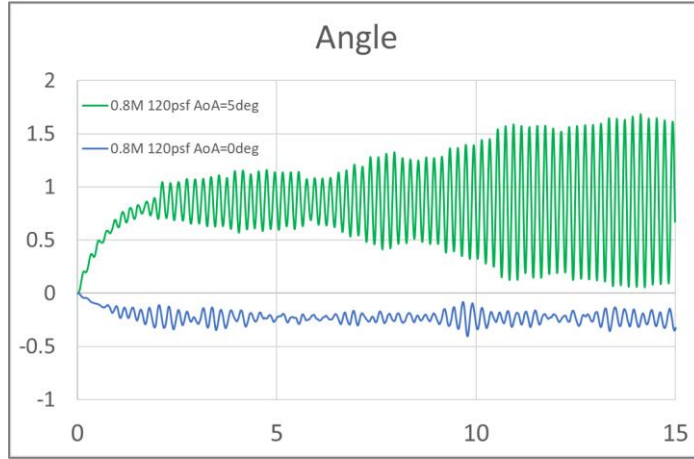


Fig. 36: Pitching angle Graph for Mach 0.8 and
Flutter Dynamic Pressure 5745 Pa (AoA 5
degrees)

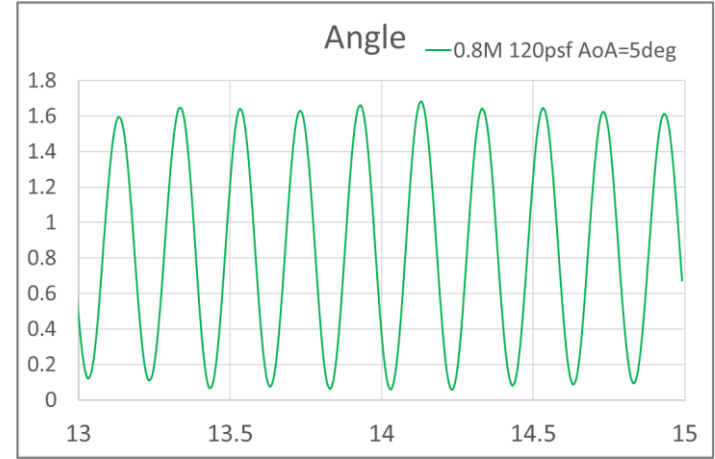


Fig.37: Pitching Angle Graph (Clear View)

At Mach 0.8, Dynamic Pressure 120 psf (5745 Pa), the pitching angle graph showed the limit cycle oscillations to occur. We see the trend in the graph is such that it diverges and then remains constant. Hence, we can conclude that the flutter is occurring in this case.

Results: Analysis result at Mach 0.8, 120 psf, AOA 0 & 5 deg

- Limit Cycle Oscillation occurs at AOA 5deg

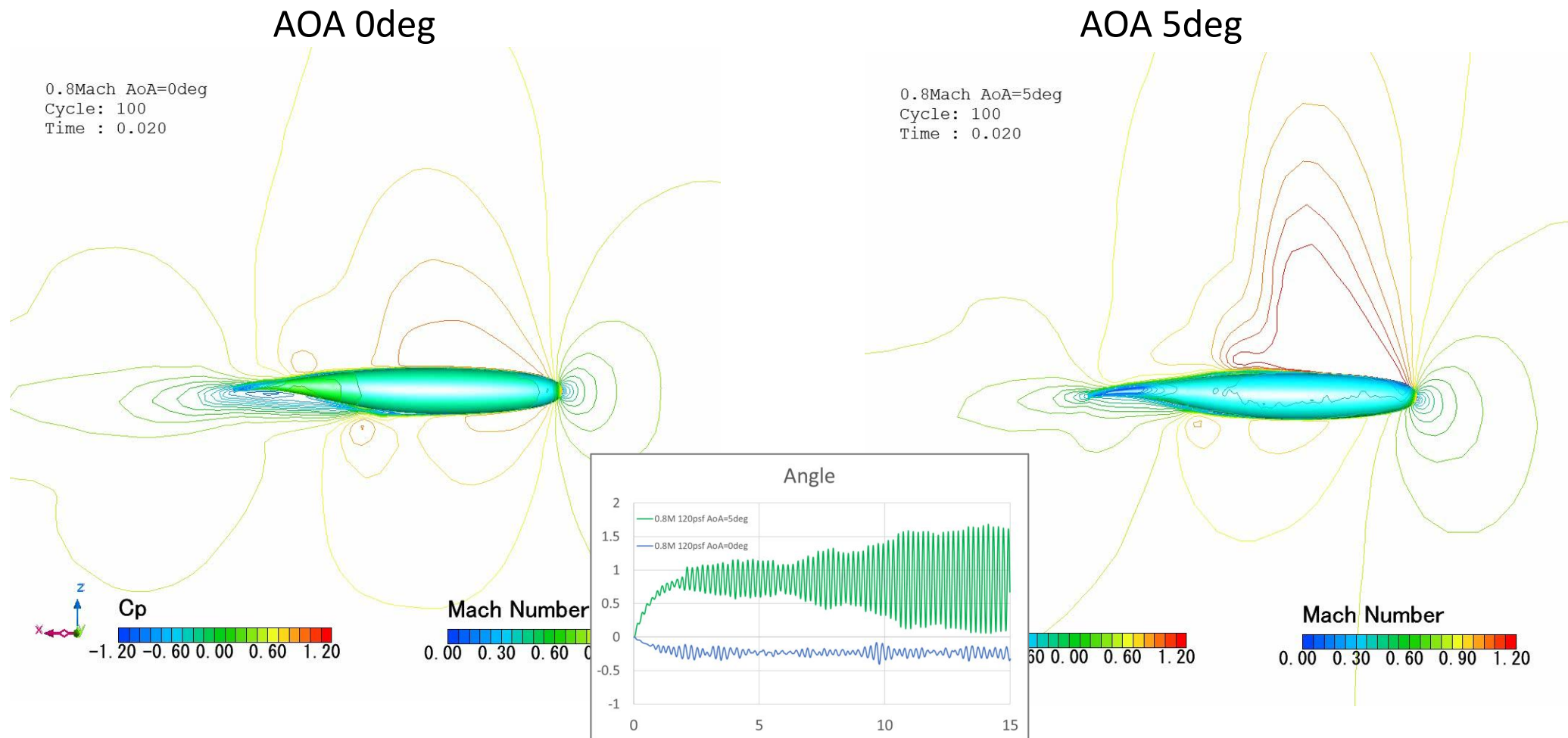


Fig. 36: Displacement Graph for Mach 0.8 and Flutter
Dynamic Pressure 5745 Pa (AoA 5 degrees)

Results: Transonic Dip at Mach 0.8

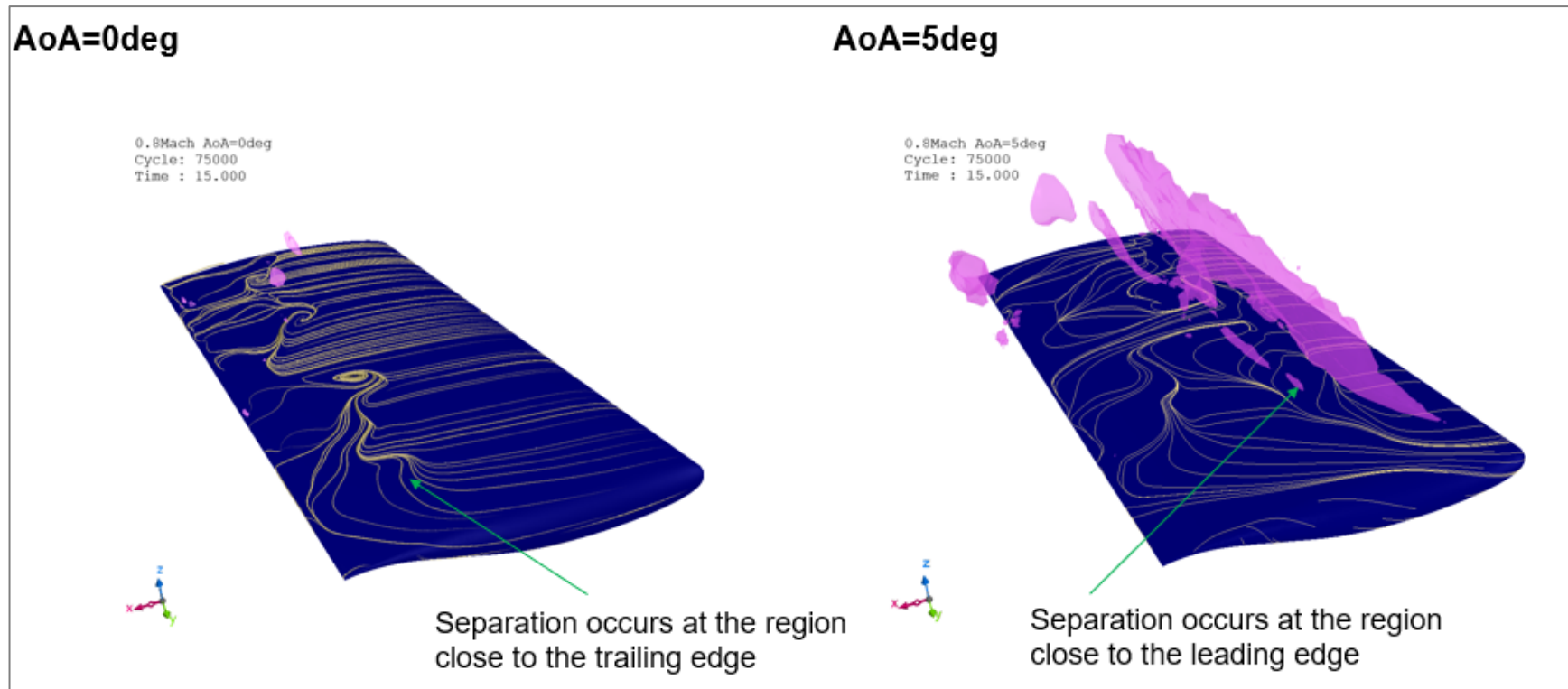


Fig. 38: Separation Contours at Mach 0.8, Dynamic Pressure 120 psf.

Also, the Figure shows that at the Angle of Attack of 0 degrees, the separation occurs close to the trailing edge, whereas, for the Angle of Attack of 5 degrees, the separation occurs close to the leading edge. Further analysis was continued to capture the Transonic Dip, for which the cases at dynamic pressure 50 psf, 80 psf, and 90 psf was performed.

Analysis result at Mach 0.8, 120 psf, AOA 5 deg

- Flutter boundary seems at 90 psf or a little smaller

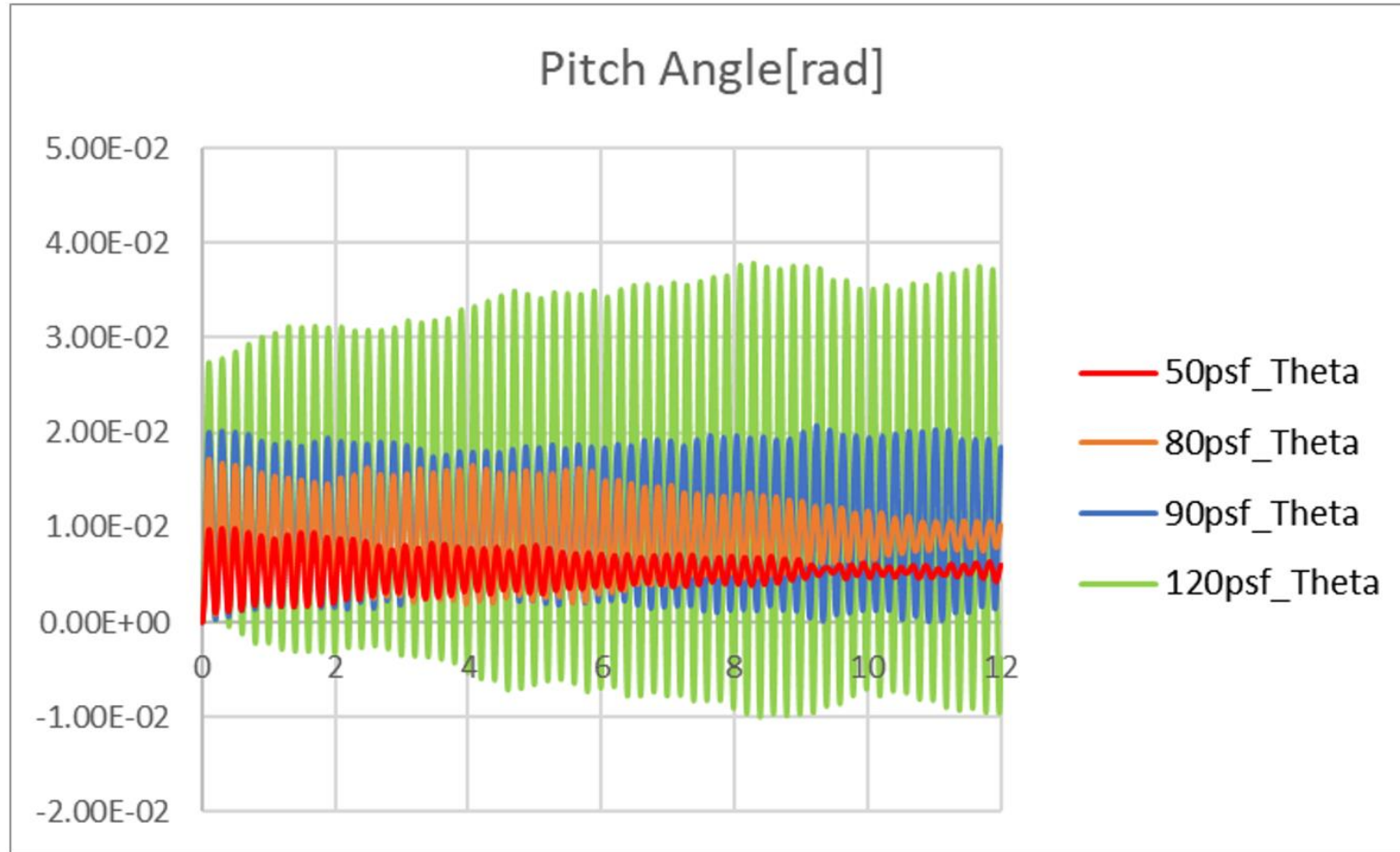


Fig.40: Pitching Angle vs. time graph

Future Work Recommendations

- ❑ Detailed Study Can be performed at even lower dynamic pressures at Mach 0.8 at an Angle of Attack of 5 degrees. This can enable us to get the exact point at which the transonic dip is occurring.
- ❑ Further Mesh resolution can be made to finer, to overcome the interference of the shock waves and the flow in the complex transonic regime.
- ❑ Further comparison can also be done with the Wind Tunnel Testing results when it is available with the High Angle Working Group.

CONCLUSION

The development of Marketing Content, as well as the development of Benchmarks on CFD problems, clearly helps in understanding the wide range of applications and the industries that are covered under the CFD domain. Industries like Aerospace, Automotive, Electronics, Building, and Architecture have gained through the highly beneficial solutions provided by CFD Cradle. The use of the software enables shortening of development time for products which is major because of many advantages of using the software like automatic mesh generation, reduction in simulation time with highly accurate results, etc.

The project on Store Separation by DSO National Laboratories is in progress. The use of overset mesh and the easy application of 6 DOF parameters in the software-enabled quick pre-processing of the problem. The results of this project will enable us to understand the viscous effects on the store trajectory.

The Co-simulation of Flutter Analysis with the use of MSC Nastran, scFLOW, and MSC CoSim enabled the easy study of Fluid-Structure interaction. The two-way coupling problem involves the transmission of pressure data and displacement data between the two solvers. With the use of Microsoft Azure, the calculation can be done faster.

BIBLIOGRAPHY AND REFERENCES

- [1] J. Heeg, P. Chwalowski, J. P. Florance, C. D. Wieseman, D. M. Schuster, and B. Perry III, "Overview of the Aeroelastic Prediction Workshop."
- [2] H. Ö. Demir, B. T. Selimhocaoğlu, and N. Alemdaroğlu, "CFD Applications in Store Separation Görkem DEMİR."
- [3] E. E. Panagiotopoulos and S. D. Kyparisis, "CFD Transonic Store Separation Trajectory Predictions with Comparison to Wind Tunnel Investigations."
- [4] Madasamy S, Thilagapathy G, and Arulagan R, "Investigation of Store Separation and Trajectory of Weapons in Military Aircraft," *International Journal of Scientific & Engineering Research*, vol. 7, no. 2, 2016, [Online]. Available: <http://www.ijser.org>
- [5] K. Jamison, "Optimised transonic store separation analyses using modern design of experiments," *International Aerospace Symposium of South Africa*, pp. 2–3, 2013.
- [6] "A. Arabshahi, D. L. Whitfield. 'A Multi-Block Approach to Solving the Three-Dimensional Unsteady Euler Equations about a Wing-Pylon-Store Configuration'. AIAA Paper 89-3401, August 1989
- [7] Donegan, "T. L. Donegan, J. H. Fox. 'Analysis of Store Trajectories from Tactical Fighter Aircraft'. AIAA Paper No. 91-0183, In proceedings of the AIAA 29th Aerospace Sciences Meeting, Reno, NV, January 7–10, 1991
- [8] K.S. Keen, "K. S. Keen. 'New Approaches to Computational Aircraft/Store Weapons Integration'. AIAA Paper No. 90-0274, In proceedings of the AIAA 28th Aerospace Sciences Meeting, Reno, NV, January 8–11, 1990
- [9] "W. L. Sickles, M. J. Rist, C. H. Morget, S. L. Keeling, K. N. Parthasarathy. 'Separation of the Pegasus XL from an L-1011 Aircraft'. AIAA Paper No. 94-3454, In proceedings of the AIAA Atmospheric Flight Mechanics Conference, August 1–3, 1994.
- [10] R. Koomullil, G. Cheng, B. Soni, R. Noack, and N. Prewitt, "Moving-body simulations using overset framework with rigid body dynamics," *Mathematics and Computers in Simulation*, vol. 78, no. 5–6, pp. 618–626, Sep. 2008, doi: 10.1016/J.MATCOM.2008.04.009.
- [11] P. Parikh, S. Pirzadeh, and N. T. Frink, "Unstructured grid solutions to a wing/pylon/store configuration," <https://doi.org/10.2514/3.46649>, vol. 31, no. 6, pp. 1291–1296, May 2012, doi: 10.2514/3.46649.
- [12] Y. E. Sunay, E. Gülay, and A. Akgül, "Numerical Simulations of Store Separation Trajectories Using the EGLIN Test," 2013.
- [13] "AePW3 | High Angle Working Group." <https://nescacademy.nasa.gov/workshops/AePW3/public/wg/highangle> (accessed May 14, 2022).
- [14] A. Jirásek, M. Dalenbring, and J. Navrátil, "Computational fluid dynamics study of benchmark supercritical wing at flutter condition," in *AIAA Journal*, 2017, vol. 55, no. 1, pp. 153–160. doi: 10.2514/1.J054916.
- [15] "cradle cfd brochure
- [16] "scFLOW User's Guide Analysis Method - 04/Nov/2021."
- [17] "Learning Center." https://learningcenter-mscemployee.sabacloud.com/Saba/Web_spf/EU2PRD0136/app/content-player?contentid=ctctx000000000219626&assignmentid=cninv00000000004305&subscriptionid=ctnsr00000000006548&launchpoint=LEARNER®id=regdw000000000062227&signOff=false&spfurl=false&backurl=me%2Flearningeventdetail%2Fcours00000000003239%3FregId%3Dregdw00000000062227%26learnerId%3Dempl00000000013260%26context%3Duser%26returnPage%3DDiscoverPortlet (accessed May 08, 2022).
- [18] "MSC Nastran 2022.1 - Online Help (HTML)." https://help.mscsoftware.com/bundle/MSC_Nastran_2022.1/page/MSC_Nastran_main.htm (accessed May 08, 2022).
- [19] "E. HEIM, 'CFD Wing/Pylon/Finned Store Mutual Interference Wind Tunnel Experiment', Arnold Engineering Development Center, AD-B152 669, September 10-17 1990.
- [20] "Store Separation Predictions for Weapon Integration on a Fighter-Type Aircraft
- [21] ARNOLD ENGINEERING DEVELOPMENT CENTER ARNOLD AFS TN and E. R. Heim, "CFD Wing/Pylon/Finned Store Mutual Interference Wind Tunnel Experiment," 1991.
- [22] *Verification and validation data for computational unsteady aerodynamics = (Données de vérification et de validation pour l'aérodynamique instationnaire numérique)*. Research and Technology Organization, 2000.
- [23] "AePW2." <https://nescacademy.nasa.gov/workshops/AePW2/public/BSCW/publications#publications> (accessed May 09, 2022).
- [24] "EXPERIMENTAL UNSTEADY PRESSURES AT FLUTTER ON THE SUPERCRITICAL WING BENCHMARK MODEL".
- [25] "AePW3 | High Angle Working Group." <https://nescacademy.nasa.gov/workshops/AePW3/public/wg/highangle> (accessed May 09, 2022).
- [26] "Arbitrary Lagrangian-Eulerian Method." http://www.me.sc.edu/research/jzu/Contents/ALE/ALE_1.htm (accessed May 09, 2022).
- [27] "Overset Mesh - Fluid Codes - Ansys Engineering Simulation." <https://fluidcodes.com/software/overset-mesh/> (accessed May 09, 2022).
- [28] M. M. Peet, "Spacecraft and Aircraft Dynamics - Lecture 9: 6DOF Equations of Motion".
- [29] "Rizzi, A: Background documentation for software & labwork. Course SD2610 Computational Aerodynamics in Aircraft Design. KTH, Dept. of Aeronautical and Vehicle Engineering, Stockholm, 2010
- [30] "Meshing Your Geometry: When to Use the Various Element Types | COMSOL Blog." <https://www.comsol.com/blogs/meshing-your-geometry-various-element-types/> (accessed May 10, 2022).
- [31] "Polyhedral mesher." <https://www.cradle-cfd.com/product/seflow/function04.html> (accessed May 10, 2022).
- [32] E. F. Toro, "Riemann solvers and numerical methods for fluid dynamics: A practical introduction," *Riemann Solvers and Numerical Methods for Fluid Dynamics: A Practical Introduction*, pp. 1–724, 2009, doi: 10.1007/B79761.
- [33] H. K. Versteeg and W. Malalasekera, "An introduction to computational fluid dynamics: the finite volume method, 1995," *Harlow-Longman Scientific & Technical, London*, vol. M, p. 503, 1996.
- [34] "Understanding The k-ε Turbulence Model – All About CFD...." <https://cfdisrael.blog/2017/04/25/understanding-the-k-%CE%B5-turbulence-model%EF%81%A5/> (accessed May 11, 2022).
- [35] A. A. Osman, A. M. Bayoumy Aly, I. El, O. E. Abdellatif, and E. E. Khallil, "Investigation of the Effect of Grid Size on External Store Separation Trajectory using CFD."
- [36] J. Navrátil, A. Jirásek, P. Hamlington, and L. Col Andrew Lofthouse, "EFFECT OF ANGLE OF ATTACK, GAS COMPOSITION AND REYNOLDS NUMBER ON FLUTTER BOUNDARY OF BENCHMARK SUPER-CRITICAL WING," 2017.
- [37] Hexagon, *MSC Nastran 2022.1*.
- [38] "MSCOne - It's time to explore a smarter way to access simulation software." <https://www.mscsoftware.com/product/mscone> (accessed Apr. 27, 2022).
- [39] A. Cenko, "Store Separation Lessons Learned (Mistakes Made)."

Acknowledgment

I would like to thank my mentor Dr. Rajesh Yadav (Associate Professor UPES), for constantly supporting me through the project and helping me understand the concept behind certain physics involved.

I would also like to thank my external mentor Dr. Karthik Sundarraj (Technical Advisor, MI India) for allowing me to intern in Hexagon and work on such projects.

I would like to sincerely thank Hatazawa Sakujiro (Senior Manager, Sales and Dealer Management, Hexagon Japan), for providing me an opportunity to work with him on the flutter prediction case. His constant guidance has helped me prepare to overcome challenges in the project.

I would like to thank Jonas Wirgart (Product Marketing Manager, Hexagon), for his constant guidance throughout my internship.

I would like to express warm gratitude to Ganesh Pawar R and Praphul T. (Technical Consultants, Hexagon India) for being such wonderful teammates and supporting and guiding me throughout the work. Without them, this would have been very challenging.

I would like to thank Katsumura Yumiko (Senior Application Engineer, Hexagon Japan), for always being ready to help with any challenges I faced with the software.

I would like to express my sincere gratitude to Pawel Chwalowski (Aeroelasticity, NASA Langley Research Center), for allowing us to work with the AePW III High Angle Working group and giving suggestions on how to improve the results.

Also, I would like to thank my course coordinator, Dr. Gurunadh Velidi, for always supporting me and guiding me throughout my post-graduation.

I will always be grateful to my institution, the University of Petroleum and Energy Studies, Dehradun for providing me with such platforms to explore the best in me.

Last, but not least, I would like to thank my family and friends for constantly motivating me to be the best version of myself.

Thank You!